*Jpn J Clin Oncol 2007;37(12)907–912*
*doi:10.1093/jjco/hym139*

# Molecular Markers and Changes of Computed Tomography Appearance in Lung Adenocarcinoma with Ground-glass Opacity

**Yukihiro Yoshida[1,4,7], Akiko Kokubu[1], Kenji Suzuki[4], Hidehiko Kuribayashi[2], Koji Tsuta[5], Yoshihiro Matsuno[5], Masahiko Kusumoto[6], Yae Kanai[3], Hisao Asamura[4], Setsuo Hirohashi[1,3] and Tatsuhiro Shibata[1,3]**

[1]Cancer Genomics Project, [2]Proteome Bioinformatics Project and [3]Pathology Division, National Cancer Center Research Institute, 5-1-1, Tsukiji, Chuo-ku, Tokyo 104-0045, [4]Thoracic Surgery Division, [5]Clinical Laboratory Division and [6]Diagnostic Radiology Division, National Cancer Center Hospital, 5-1-1, Tsukiji, Chuo-ku, Tokyo 104-0045, Japan

Received March 31, 2007; accepted July 5, 2007; published online December 18, 2007

**Background:** High-resolution computed tomography (HRCT) of lung adenocarcinoma at early stage shows pure ground-glass opacity (GGO) and most cases of pure GGO remain stable during follow-up. There is no consensus on the strategy for follow-up. Identification of the molecular mechanisms that are associated with the natural history of lung adenocarcinoma should provide useful information.
**Methods:** Twenty-three lung adenocarcinomas that were followed-up for more than 6 months pre-operatively by HRCT were included in this study. Patterns of radiological changes during the follow-up period were classified into three groups; type 1, pure GGO without consolidation; type 2, appearance or increase in consolidation within pure GGO; type 3, consolidation without pure GGO. Mutational analysis of the epidermal growth factor receptor (EGFR) and K-ras genes and immunohistochemical staining of p53 protein were performed.
**Results:** EGFR mutations were found in 17 cases (74%), and there was no K-ras mutation. Positive staining of p53 was found in 8 cases (35%). As for radiological findings during the follow-up period, the frequencies of EGFR mutations and positive p53 staining were 67 and 0% in type 1 ($n = 9$), 89 and 44% in type 2 ($n = 9$) and 60 and 80% in type 3 ($n = 5$).
**Conclusions:** EGFR mutations were frequently found in lung adenocarcinoma with GGO on HRCT in this study. Inactivation of p53 may be associated with the appearance of central consolidation within pure GGO on HRCT which reflects invasive features and may be useful as a molecular marker during the follow-up of pure GGO.

*Key words: lung neoplasms – tomography – spiral computed receptor – epidermal growth factor – tumor suppressor protein p53 – adenocarcinoma – bronchioloalveolar*

## INTRODUCTION

Due to recent advances in computed tomography (CT) imaging and the prevalence of lung cancer screening with the use of helical CT, the frequency of small and early lung cancers which are invisible on chest X-ray is increasing in Japan (1). Most pure ground-glass opacity (GGO) lesions detected by helical CT are stable in size during the follow-up period and are pathologically atypical adenomatous hyperplasia (AAH) or bronchioloalveolar carcinoma (BAC), which shows lepidic growth without invasion (2). Although the prognosis after surgical resection is excellent (2), some lesions with pure GGO progress rapidly (3). Although intensive and careful follow-up is required for pure GGO, it remains unknown how long and how often these should be followed.

A hypothesis of multistage carcinogenesis of lung adenocarcinoma was proposed, but it is still unclear how the lesion progresses over time in terms of radiological, pathological and molecular characteristics. Since it is technically and ethically difficult to obtain tissue samples from these lesions, most studies that have sought to reveal the natural history of lung adenocarcinoma were based on radiological findings during the pre-operative follow-up period (3–6). None of them examined the molecular

For reprints and all correspondence: Tatsuhiro Shibata, Cancer Genomics Project, National Cancer Center Research Institute, 5-1-1, Tsukiji, Chuo-ku, Tokyo 104-0045, Japan. E-mail: tashibat@ncc.go.jp

[7]Present address: Department of Thoracic Surgery, The University of Tokyo Hospital, Tokyo, Japan

markers that are associated with the natural history of lung adenocarcinoma.

Recently, somatic mutations of the epidermal growth factor receptor (EGFR) gene were reported in lung adenocarcinoma (7,8). They have also been found in AAH and BAC (9,10). Our previous study revealed that EGFR mutations occur in the early stage of lung adenocarcinoma, such as AAH and BAC, suggesting that they play an important role in disease progression, whereas AAH with K-ras mutations stays indolent (10). Consequently, we hypothesized that these two mutually exclusive mutations might determine the natural history of pure GGO lesions.

Identification of the molecular mechanisms that affect the biological behavior of GGO lesions may offer useful information for determining the appropriate follow-up strategy for pure GGO lesions. We examined the radiological changes and genetic aberrations for lesions that were followed-up preoperatively to clarify the molecular markers that are associated with the natural history of pure GGO.

## PATIENTS AND METHODS

This is a retrospective cohort study. This study was approved by the institutional review board (date of IRB approval: 30 September 2005). First, we selected patients with more than 6 months interval between their first visit to the hospital and the date of the operation by using the National Cancer Center Hospital Thoracic Surgery Division Database, which is an electronic prospective database for surgical records. All charts of listed patients were reviewed to obtain further clinical and pathological information and to select appropriate cases that fulfilled all the following criteria; surgical cases from January 2000 to December 2004, pathological diagnosis of primary lung adenocarcinoma and cases that were followed-up for >6 months before the operation using high-resolution CT (HRCT). The aim of this study is to clarify the natural history of lung adenocarcinoma in view of radiological, pathological and molecular findings, so we excluded other potential etiologies for GGO such as AAH, infection, respiratory bronchiolitis which had been followed up for >6 months using HRCT and then surgically resected. We also excluded mucinous BAC and mucin-producing adenocarcinoma of the lung. Twenty-three cases were included in the study. Ten patients were followed up because of pure GGO lesion with its size of 15 mm or less, to which surgical resection would not be indicated until radiological changes such as increase in size or attenuation, appearance of consolidation were observed. Other reasons were diagnosis of inflammation on HRCT at the initial presentation ($n = 4$), the previous history of lung surgery in the contralateral side ($n = 4$), other malignancy under treatment ($n = 2$) and patient's request for further follow-up ($n = 3$). The median follow-up interval between the initial and last HRCT scan before the operation was 18 (6–62) months.

### Radiological Diagnosis

CT was performed on helical or multidetector scanners (X-Vigor, TCT-900S units or Aquilion V-detector; Toshiba Medical Systems, Tokyo, Japan) as described previously (11,12). The helical technique in 14 examinations consisted of 10.0-mm collimation for individual scans of the entire lung [120 kV (peak), 150 mA] and reconstruction using a standard algorithm. Additional thin-section CT images at the level of the lesion were obtained using 2.0-mm collimation, a 20-cm field of view, 120 kVp and 200 mA per rotation, 1.0-s gantry rotation and a high spatial frequency reconstruction algorithm. The remaining 32 examinations were evaluated on a multidetector CT scanner using axial 2.0-mm × 4 modes (four images per gantry rotation), 120 kVp, 200 mA, and 0.5-s scanning time. Thin section CT images were obtained using 2.0-mm sections reconstructed at 2.0-mm intervals using a high spatial frequency algorithm and were retrospectively retargeted to each lung with a 20-cm field of view. In 17 examinations, nonionic iodinated contrast material was administered intravenously. The scans were viewed on standard mediastinal window setting (window level, 70 H; window width, 400 H) and lung window setting (window level, −600 H; window width, 1500–2000 H).

GGO and consolidation were defined based on our previous study (13). A GGO appearance on HRCT corresponds to lepidic growth of cancer cells along alveolar walls (BAC features), whereas the proportion of consolidation is a predictor of pathological invasiveness (13). Patterns of radiological changes during the follow-up period were classified into three types (Fig. 1): type 1, pure GGO without consolidation during the follow-up period; type 2, appearance or increase in consolidation within pure GGO during the follow-up period; type 3, consolidation without pure GGO during the follow-up period. A board-certified general thoracic surgeon who was unaware of clinical and experimental information (K.S.) diagnosed the findings.

A board-certified clinician who was unaware of clinical and experimental information (H.K.) encircled the lesion using the segmented line selection tool in Image J software and measured the largest diameter and perpendicular size of

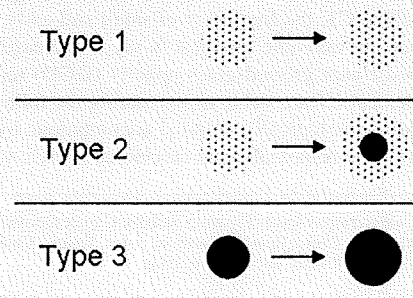


**Figure 1.** Schema of patterns of radiological changes during the follow-up period in this study.

the lesion (14). Corresponding slices in the initial and last HRCT examination were used. Tumor doubling time (TDT) was calculated using the formula proposed by Schwarts (15).

### Mutational Analysis

Seven methanol-fixed and 16 formalin-fixed archives were used for mutational analysis of exons 18, 19 and 21 of the EGFR gene and exon 2 of the K-ras gene. Tumor DNA was purified by laser-captured microdissection (16). Information on primer sequences is available on request. Polymerase chain reactions and direct sequencing were performed as described previously (10). Peripheral lung tissue without cancer cells was used as a reference.

### Pathological Diagnosis and Immunohistochemical Study

The pathological diagnosis of lung adenocarcinoma was categorized into four types according to the proposal by Ebright et al. (17): adenocarcinoma without BAC features, adenocarcinoma with BAC features (AwBF), BAC with focal invasion (BwFI) and pure BAC (PBAC).

Immunohistochemical staining of p53 was performed using a mouse primary antibody (1:100 dilution; clone DO7, Dako A/S, Glostrup, Denmark) and the avidin biotin complex method as described previously (18). A board-certified pathologist (K.T.) who was unaware of clinical and experimental information evaluated staining according to our previous criteria; +, when the proportion of tumor cells with definitely brownish nuclear staining was >20%; ±, when stained tumor cells were scattered, representing <20% of the tumor cells; −, when p53-positive cells were completely absent or seen only occasionally (19).

### Clinical Information

Patient charts were reviewed to obtain clinical information. Patients who had quit smoking at least 1 year before the operation were defined as former smokers (20). Multiple lung cancers were discriminated from pulmonary metastases by applying the criteria proposed by Martini and Melamed (21). The TNM staging system revised in 1997 was adopted (22). All cases were cT1N0M0 and pT1N0M0. Surgical procedures were lobectomy in 11 cases, segmentectomy in 4 cases and wide wedge resection in 8 cases. The median follow-up period after the operation was 21 (9–65) months. Recurrence in the mediastinum was observed 12 months after the operation in one case with metachronous multiple lung cancers. The other 22 cases were alive without recurrence.

## RESULTS

The 23 lesions are summarized in Table 1, and representative cases are shown in Figs. 2–5. Increase in size of 2 mm or more during follow-up period was observed in 10 cases (1 case was type 1, 5 were type 2 and 4 were type 3) and decrease in size of 2 mm or more was observed in one case of type 2 radiological classifications. The 8 men and 15 women had a median age of 66 years (37–77). Three were current smokers, 6 were former smokers and 14 were never smokers. There were seven cases of multiple lung cancers (metachronous in two cases and synchronous in five cases) and two cases were type 1, four were type 2 and 1one was type 3. Patients with type 3 radiological classification tended to have shorter interval between the initial and last HRCT examination and TDT of less than 24 months (Table 1).

EGFR mutations were found in 17 cases (74%), and all were somatic mutations (Table 2). There was no K-ras mutation in any of the 23 cases. Immunohistochemical staining of p53 was positive in eight cases (35%). Staining patterns were diffuse in all cases. Positive staining was

**Table 1.** Summary of clinical, pathological and radiological results

| | Radiological findings | | |
|---|---|---|---|
| | Type 1 | Type 2 | Type 3 |
| Age, years | | | |
| Median | 59 | 69 | 68 |
| Range | 40–75 | 53–77 | 37–74 |
| Sex | | | |
| Female | 7 | 6 | 2 |
| Male | 2 | 3 | 3 |
| Smoking history | | | |
| Never | 6 | 4 | 4 |
| Former/current | 3 | 5 | 1 |
| Histological diagnosis | | | |
| PBAC | 3 | 2 | 0 |
| BwFI | 6 | 7 | 3 |
| AwBF | 0 | 0 | 2 |
| Size*, cm | | | |
| Median | 1.4 | 1.6 | 1.6 |
| Range | 0.6–1.8 | 0.8–2.8 | 1.5–2.3 |
| Interval**, months | | | |
| Median | 20 | 16 | 12 |
| Range | 6–32 | 8–62 | 6–28 |
| TDT | | | |
| 0 < TDT < 24 | 3 | 3 | 4 |
| 24 < TDT | 2 | 4 | 1 |
| TDT < 0*** | 4 | 2 | 0 |

PBAC, pure bronchiolo-alveolar carcinoma; BwFI, BAC with focal invasion; AwBF, adenocarcinoma with BAC features; TDT, tumor doubling time; HRCT, high-resolution computed tomography.
*Size at the last HRCT examination.
**Interval between the initial and last HRCT examination.
***Reduction in volume during the follow-up period.

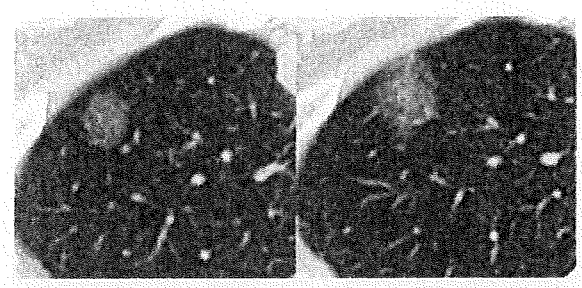

**Figure 2.** (Left: initial high-resolution computed tomography (HRCT): right: last HRCT; type 1 radiological finding) 66-year-old female, never smoker, 28-month interval; pure bronchioloalveolar carcinoma with del L747-T751.

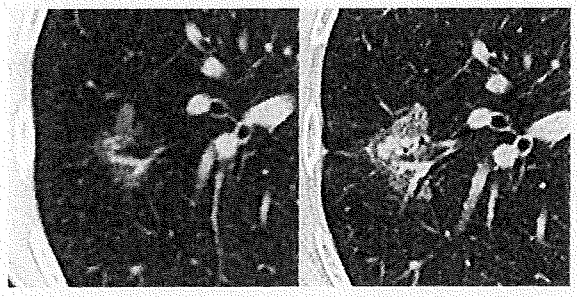

**Figure 3.** (Left: initial HRCT, right: last HRCT; type 2 radiological finding) 73-year-old female, never smoker, 11-month interval; BFWI with L858R.

observed both in the periphery of the lesion where cancer cells are lining along the alveolar walls and central areas where cancer cells are invading into the stroma.

The relationships between radiological findings, EGFR mutations and p53 staining are shown in Table 3. EGFR mutations were found in 67% of Type 1, 89% of Type 2 and 60% of Type 3. There was no trend between EGFR mutations and patterns of radiological changes during the follow-up period. The frequency of EGFR mutations was above 60% in all groups. The frequency of p53-positive was 44% in type 2 and 80% in type 3, in contrast to 0% in type 1. There was a trend between positive p53 immunohistochemistry and patterns of radiological changes during the follow-up period.

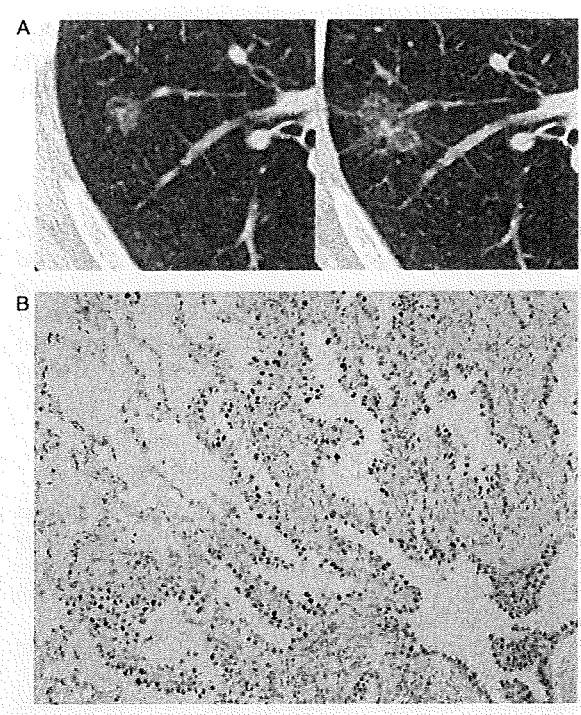


**Figure 4.** (A) (left: initial HRCT; right: last HRCT; type 2 radiological finding) 59-year-old male, former smoker, 62-month interval; BAC with focal invasion with del E746-A 750. (B) Immunohistochemical staining of p53 in the same case as in (A). p53 immunohistochemical staining showed reactivity in most tumor nuclei, but not in normal alveolar cells (hematoxylin and eosin staining, original magnification ×100).

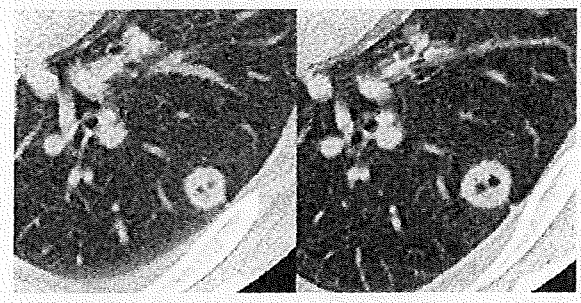

**Figure 5.** (Left: initial HRCT; right: last HRCT; type 3 radiological finding) 37-year-old male, never smoker, 6-month interval; adenocarcinoma with BAC features with wild type.

## DISCUSSION

Several studies have been conducted to reveal the natural history of lung adenocarcinoma based on radiological findings during the pre-operative follow-up period (3–6). Most of them were based on the screening with low-dose CT, conventional CT with a 10 mm interval, which was not appropriate for a detailed and precise analysis of radiological findings. No study has ever examined molecular markers. To clarify the natural history of lung adenocarcinoma in view of radiological, pathological and molecular findings, we examined selected cases of patients who were followed-up for at least 6 months using HRCT pre-operatively and investigated the molecular markers that may be associated with the pattern of radiological changes during the follow-up period.

Biological behaviors of pure GGO may be determined by either initial aberrations of multistage carcinogenesis or additional aberrations during its progression. Since we

**Table 2.** EGFR mutations detected in the present study

| Exons | Amino acids | Nucleotides | No. of patients |
|---|---|---|---|
| Exon 19 | del E746-A750 | del 2235-2249 | 1 |
| | del E746-A750 | del 2236-2250 | 6 |
| | del E746-T751insS | del2236-2251 + insT | 1 |
| | del L747-T751 | del 2239-2253 | 3 |
| Exon 21 | L858R | Substitution of G for T at nucleotide 2573 | 6 |

EGFR, epidermal growth factor receptor.

**Table 3.** EGFR mutations, immunohistochemical staining of p53 and patterns of radiological changes during the follow-up period

| | Number | EGFR mutation | Deletions in Exon 19 | L858R | Positive p53 IHC |
|---|---|---|---|---|---|
| Type 1 | 9 | 67% | 4 | 2 | 0% |
| Type 2 | 9 | 89% | 5 | 3 | 44% |
| Type 3 | 5 | 60% | 2 | 1 | 80% |

IHC, immunohistochemistry.

previously demonstrated that both EGFR and K-ras mutations were early events in lung adenocarcinoma (10), we examined whether these mutations were associated with the natural history of pure GGO.

We detected EGFR mutations in 17 cases (74%). Such a high incidence of EGFR mutations was probably due to the fact that all of the lesions in our study were AwBF, which frequently harbor EGFR mutations (20). We consistently observed EGFR mutations in most of the lesions with a GGO appearance (78% in types 1 and 2).

We classified lung adenocarcinoma in terms of the pattern of radiological changes during the follow-up period into three types and investigated differences between them from a molecular perspective. In our study, we should consider that the patterns of radiological changes during the follow-up period may not be distinct from each other, but rather they might be a transient finding in multistage carcinogenesis of lung adenocarcinoma. Lesions with a type 1 radiological classification might progress to type 2 and eventually type 3 during a long follow-up. The frequent EGFR mutations in type 1 (67%) suggested that they play a role in initiation (Table 3). However, EGFR mutations failed to distinguish the radiological classifications from each other, in contrast to our hypothesis, and this suggested that such mutations have little association with the progressive behavior of pure GGO.

There was no case of positive p53 staining in type 1 in our study, in contrast to type 2 (44%) and type 3 (80%). Our result suggests that the inactivation of p53 might be associated with the appearance of consolidation within a pure GGO lesion on HRCT which reflects invasive features of the lesion. Therefore, p53 should be a useful biomarker for determining the follow-up strategy for pure GGO lesions. The detection of serum p53 auto-antibodies, e.g. might complement a radiological follow-up, prevent the unnecessary exposure to X-rays and even precede HRCT findings to determine the appropriate timing for surgical intervention without delay (23,24). Previous study by others also demonstrated that among lung AwBF, the frequency of positive p53 staining was low in PBAC, whereas it increased in accordance with invasive features and they concluded that p53 played an important role in the progression of lung adenocarcinoma, although their study did not take into account periodic changes (19).

Since lung nodules that are stable for 2 years are considered to be benign, we defined a TDT cut-off value of 2 years in Table 1 (25). However, we have to be careful when applying TDT to lesions with GGO, in which cancer cells grow in a lepidic fashion without filling alveolar spaces. In addition, some lung adenocarcinomas retract the surrounding structures and shrink in size during their progression, which makes it difficult to interpret TDT (3).

Our study has several limitations, such as the small number of patients, the short follow-up between the initial and last HRCT examination and possible inter-observer variability of HRCT findings. Furthermore, the results may have been biased since we only considered surgically resected cases and we have no data on genetic aberrations for pure GGO that is stable and followed-up without surgical resection. Although K-ras mutations are frequently found in mucinous BAC or mucin-producing adenocarcinoma of the lung (26), we found no K-ras mutation in this study. The progression of multistage carcinogenesis in lung adenocarcinoma with K-ras mutations remains unclear.

It is important that we understand multistage carcinogenesis of lung adenocarcinoma to identify molecular biomarkers which can discriminate pure GGO lesions which progress from those which stay indolent. We found that the inactivation of p53 might be associated with the appearance of central consolidation within pure GGO on HRCT in this study. These markers should offer useful information for determining the appropriate strategy regarding the interval and duration of follow-up for pure GGO lesions detected by helical CT.

## FUNDING

This work was supported in part by Public Trust Haraguchi Memorial Cancer Research Fund, a grant-in-aid for the Comprehensive 10-Year-Strategy for Cancer Control from the Ministry of Health, Labor and Welfare, Japan and the Program for Promotion of Fundamental Studies in Health Sciences of the National Institute of Biomedical Innovation (NiBio), Japan.

**Conflict of interest statement**

None declared.

## References


1. Kaneko M, Eguchi K, Ohmatsu H, Kakinuma R, Naruke T, Suemasu K, et al. Peripheral lung cancer: screening and detection with low-dose spiral CT versus radiography. *Radiology* 1996;201:798–802.
2. Nakata M, Sawada S, Saeki H, Takashima S, Mogami H, Teramoto N, et al. Prospective study of thoracoscopic limited resection for ground-glass opacity selected by computed tomography. *Ann Thorac Surg* 2003;75:1601–5.
3. Kakinuma R, Ohmatsu H, Kaneko M, Kusumoto M, Yoshida J, Nagai K, et al. Progression of focal pure ground-glass opacity detected by low-dose helical computed tomography screening for lung cancer. *J Comput Assist Tomogr* 2004;28:17–23.
4. Aoki T, Nakata H, Watanabe H, Nakamura K, Kasai T, Hashimoto H, et al. Evolution of peripheral lung adenocarcinomas: CT findings correlated with histology and tumor doubling time. *AJR Am J Roentgenol* 2000;174:763–8.
5. Kodama K, Higashiyama M, Yokouchi H, Takami K, Kuriyama K, Kusunoki Y, et al. Natural history of pure ground-glass opacity after long-term follow-up of more than 2 years. *Ann Thorac Surg* 2002;73:386–92.
6. Takashima S, Maruyama Y, Hasegawa M, Yamanda T, Honda T, Kadoya M, et al. CT findings and progression of small peripheral lung neoplasms having a replacement growth pattern. *AJR Am J Roentgenol* 2003;180:817–26.
7. Lynch TJ, Bell DW, Sordella R, Gurubhagavatula S, Okimoto RA, Brannigan BW, et al. Activating mutations in the epidermal growth factor receptor underlying responsiveness of non-small-cell lung cancer to gefitinib. *N Engl J Med* 2004;350:2129–39.
8. Paez JG, Janne PA, Lee JC, Tracy S, Greulich H, Gabriel S, et al. EGFR mutations in lung cancer: correlation with clinical response to gefitinib therapy. *Science* 2004;304:1497–500.
9. Yatabe Y, Kosaka T, Takahashi T, Mitsudomi T. EGFR mutation is specific for terminal respiratory unit type adenocarcinoma. *Am J Surg Pathol* 2005;29:633–9.
10. Yoshida Y, Shibata T, Kokubu A, Tsuta K, Matsuno Y, Kanai Y, et al. Mutations of the epidermal growth factor receptor gene in atypical adenomatous hyperplasia and bronchioloalveolar carcinoma of the lung. *Lung Cancer* 2005;50:1–8.
11. Oshiro Y, Kusumoto M, Matsuno Y, Asamura H, Tsuchiya R, Terasaki H, et al. CT findings of surgically resected large cell neuroendocrine carcinoma of the lung in 38 patients. *AJR Am J Roentgenol* 2004;182:87–91.
12. Tateishi U, Muller NL, Johkoh T, Maeshima A, Asamura H, Satake M, et al. Mucin-producing adenocarcinoma of the lung: thin-section computed tomography findings in 48 patients and their effect on prognosis. *J Comput Assist Tomogr* 2005;29:361–8.
13. Asamura H, Suzuki K, Watanabe S, Matsuno Y, Maeshima A, Tsuchiya R. A clinicopathological study of resected subcentimeter lung cancers: a favorable prognosis for ground glass opacity lesions. *Ann Thorac Surg* 2003;76:1016–22.
14. Abramoff MD, Magelhaes PJ, Ram SJ. Image Processing with Image J. *Biophotonics International* 2004;11:36–42.
15. Schwarts M. A biomathematical approach to clinical tumor growth. *Cancer* 1961;14:1272–94.
16. Emmert-Buck MR, Bonner RF, Smith PD, Chuaqui RF, Zhuang Z, Goldstein SR, et al. Laser capture microdissection. *Science* 1996;274:998–1001.
17. Ebright MI, Zakowski MF, Martin J, Venkatraman ES, Miller VA, Bains MS, et al. Clinical pattern and pathologic stage but not histologic features predict outcome for bronchioloalveolar carcinoma. *Ann Thorac Surg* 2002;74:1640–6.
18. Etoh T, Kanai Y, Ushijima S, Nakagawa T, Nakanishi Y, Sasako M, et al. Increased DNA methyltransferase 1 (DNMT1) protein expression correlates significantly with poorer tumor differentiation and frequent DNA hypermethylation of multiple CpG islands in gastric cancers. *Am J Pathol* 2004;164:689–99.
19. Terasaki H, Niki T, Matsuno Y, Yamada T, Maeshima A, Asamura H, et al. Lung adenocarcinoma with mixed bronchioloalveolar and invasive components: clinicopathological features, subclassification by extent of invasive foci, and immunohistochemical characterization. *Am J Surg Pathol* 2003;27:937–51.
20. Takano T, Ohe Y, Sakamoto H, Tsuta K, Matsuno Y, Tateishi U, et al. Epidermal growth factor receptor gene mutations and increased copy numbers predict gefitinib sensitivity in patients with recurrent non-small-cell lung cancer. *J Clin Oncol* 2005;23:6829–37.
21. Martini N, Melamed MR. Multiple primary lung cancers. *J Thorac Cardiovasc Surg* 1975;70:606–12.
22. Mountain CF. Revisions in the international system for staging lung cancer. *Chest* 1997;111:1710–7.
23. Lubin R, Zalcman G, Bouchet L, Tredaniel J, Legros Y, Cazals D, et al. Serum pp53 antibodies as early markers of lung cancer. *Nat Med* 1995;1:701–2.
24. Mitsudomi T, Suzuki S, Yatabe Y, Nishio M, Kuwabara M, Gotoh K, et al. Clinical implications of p53 autoantibodies in the sera of patients with non-small-cell lung cancer. *J Natl Cancer Inst* 1998;90:1563–8.
25. MacMahon H, Austin JH, Gamsu G, Herold CJ, Jett JR, Naidich DP, et al. Fleischner Society: Guidelines for management of small pulmonary nodules detected on CT scans: a statement from the Fleischner Society. *Radiology* 2005;237:395–400.
26. Kobayashi T, Tsuda H, Noguchi M, Hirohashi S, Shimosato Y, Goya T, et al. Association of point mutation in c-Ki-ras oncogene in lung adenocarcinoma with particular reference to cytologic subtypes. *Cancer* 1990;66:289–94.

# Gene Amplification and Overexpression of *PRDM14* in Breast Cancers

Noriko Nishikawa,[1,2] Minoru Toyota,[1,3,5] Hiromu Suzuki,[4] Toshio Honma,[2] Tomoko Fujikane,[1,2] Tousei Ohmura,[2] Toshihiko Nishidate,[2] Mutsumi Ohe-Toyota,[1] Reo Maruyama,[3] Tomoko Sonoda,[4] Yasushi Sasaki,[1] Takeshi Urano,[6] Kohzoh Imai,[3] Koichi Hirata,[2] and Takashi Tokino[1]

[1]Department of Molecular Biology, Cancer Research Institute, [2]First Department of Surgery, [3]First Department of Internal Medicine, and [5]Department of Public Health, Sapporo Medical University, Sapporo, Japan; [5]PRESTO, Japan Science and Technology Corporation, Kawaguchi, Japan; and [6]Department of Biochemistry, Shimane University Faculty of Medicine, Izumo, Japan

## Abstract

**Several genes that encode PR (*P*RDI-BF1 and *R*IZ) domain proteins (PRDM) have been linked to human cancers. To explore the role of the PR domain family genes in breast carcinogenesis, we examined the expression profiles of 16 members of the *PRDM* gene family in a panel of breast cancer cell lines and primary breast cancer specimens using semi-quantitative real-time PCR. We found that *PRDM14* mRNA is overexpressed in about two thirds of breast cancers; moreover, immunohistochemical analysis showed that expression of PRDM14 protein is also up-regulated. Analysis of the gene copy number revealed that *PRDM14* is a target of gene amplification on chromosome 8q13, which is a region where gene amplification has frequently been detected in various human tumors. Introduction of *PRDM14* into cancer cells enhanced cell growth and reduced their sensitivity to chemotherapeutic drugs. Conversely, knockdown of *PRDM14* by siRNA induced apoptosis in breast cancer cells and increased their sensitivity to chemotherapeutic drugs, suggesting that up-regulated expression of *PRDM14* may play an important role in the proliferation of breast cancer cells. That little or no expression of *PRDM14* is seen in noncancerous tissues suggests that *PRDM14* could be an ideal therapeutic target for the treatment of breast cancer.** [Cancer Res 2007; 67(20):9649–57]

## Introduction

In the past few years, much progress has been made toward a better understanding of the molecular mechanisms involved in breast cancer. Among these are mechanisms by which gene expression is regulated, including the reversible modification of core histones through acetylation, phosphorylation, or methylation (1). The methylation of lysine residues on histone tails is catalyzed by enzymes containing a conserved Su(var)3-9, Enhancer-of-zeste and Trithorax (SET) domain. Such histone methyltransferases control epigenetic inheritance through transfer of methyl groups from the methyl donor *S*-adenosylmethionine to basic residues on histones (2). Methylation events driven by these enzymes have, in some cases, been implicated in gene silencing and carcinogenesis. For instance, up-regulated expression of one of the polycomb group genes, EZH2, which encodes a protein with H3-K27 histone methyltransferase activity, is associated with a high cell proliferation rate and aggressive breast cancers (3). The expression of SMYD3, which also contains a SET domain, also is up-regulated in human breast cancer (4), and the variable number of tandem repeats polymorphism in the SMYD3 gene promoter region is associated with an increased risk of breast cancer (5, 6).

The *P*RDI-BF1 and *R*IZ homologous (PR) domain proteins (PRDM) are a subclass of the SET domain proteins that was first noted in the homologous region shared by RIZ1/PRDM2 and BLIMP1/PRDM1 (7) and also show homology with SET domain proteins related to known histone methyltransferases (8, 9). Although the role of PRDMs in modulating transcription remains unclear, recent studies indicate that they do play a role in tumorigenesis. For instance, both *RIZ1/PRDM2*, which encodes a Rb-binding protein, and *BLIMP1/PRDM1*, which encodes a c-Myc transcription repressor and promotes B-lymphocyte maturation (7, 10–13), induce growth arrest and exhibit proapoptotic activities (12, 14). In addition, the *MDS1-EVI1/PRDM3* gene is commonly mutated in myeloid leukemia (15), whereas the *PMF1/PRDM4* gene is located at a tumor suppressor locus on 12q23-q24 (16), and its overexpression inhibits DNA synthesis (17). Finally, expression of both *PRDM5* and *RIZ1/PRDM2* is commonly silenced through CpG island promoter DNA methylation in several cancer types including breast, ovarian, and liver cancers (18, 19).

In the present study, we examined the expression profile of PR domain family genes in breast cancers. We found that among the 16 members, *PRDM14* is frequently overexpressed and is amplified in breast cancer. Our data suggest that PRDM14 could harbor an oncogenic property and function as a novel molecular target in the treatment of these tumors.

## Materials and Methods

**Cell lines and specimens.** Seven breast cancer cell lines (MCF7, MB231, MB435, MB436, MB468, SKBr-3, and T47D), 7 gastric cancer cell lines (MKN7, MKN28, MKN74, AZ521, KatoIII, JRST, and SNU638), and 15 ovarian cancer cell lines (SKOV-3, OVCA-3, PA-1, Caov-3, MH, KURA, AMOC-2, MCAS, KF, KFr, HTBOA, TOV-21G, SW626, TOV-112D, and OV-90) were obtained from the American Type Culture Collection or the Japanese Collection of Research Bioresources. All cell lines were cultured in appropriate medium supplemented with 10% fetal bovine serum and incubated under a 5% $CO_2$ atmosphere at 37°C. In addition, 55 breast cancer specimens and 8 breast tissue samples from areas adjacent to tumors were obtained from Sapporo Medical University Hospital at surgery and stored

**Note:** Supplementary data for this article are available at Cancer Research Online (http://cancerres.aacrjournals.org/).

**Requests for reprints:** Minoru Toyota, First Department of Internal Medicine, Sapporo Medical University, South 1, West 16, Chuo-ku, Sapporo 060-8543, Japan. Phone: 81-11-611-2111, ext. 3211; Fax: 81-11-618-3313; E-mail: mtoyota@sapmed.ac.jp.



doi:10.1158/0008-5472.CAN-06-4111

at −80°C. In accordance with institutional guidelines, all patients gave informed consent before collection of the specimens. Genomic DNA was extracted using the phenol/chloroform method. Total RNA was extracted from cell lines using Trizol (Life Technologies, Inc.) according to the manufacturer's instructions.

**Real-time PCR.** The reverse transcriptase reaction was carried out with 5 μg of total RNA using a SuperScript II First-Strand Synthesis System (Invitrogen, Inc.) with random primers. Relative real-time PCR for detection of gene expression levels was carried out using an ABI PRISM 7900HT Sequence Detection System (Applied Biosystems). Primers and probes were purchased from Applied Biosystems. The reaction mixture (total volume 20 μL) contained ~10 ng of cDNA, primers, and probes at final concentrations of 300 and 200 nmol/L, respectively, as well as commercial reagents (Universal Master Mix, Applied Biosystems). Relative levels of gene expression were quantified using the ΔΔCt method, which results in a ratio of target gene expression to equally expressed housekeeping genes. For calibration, the ratio in a sample of normal breast tissue from an area adjacent to the tumor was determined. Glyceraldehyde-3-phosphate dehydrogenase (*GAPDH*) was chosen as the housekeeping gene. The primer/probe sets used were as follows: *PRDM1*, Hs00153357; *PRDM2*, Hs00210612; *PRDM3*, Hs00602795; *PRDM4*, Hs00183764; *PRDM5*, Hs00218855; *PRDM6*, Hs01373000; *PRDM7*, Hs00364862; *PRDM8*, Hs00220274; *PRDM9*, Hs00360639; *PRDM10*, Hs00360651; *PRDM11*, Hs00220293; *PRDM12*, Hs00222080; *PRDM13*, Hs00222082; *PRDM14*, Hs00225842; *PRDM15*, Hs00411330; *PRDM16*, Hs00223161_A1; *CEACAM6*, Hs00366002_m1; *CEACAM7*, Hs00185152_m1; *CCDC3*, Hs00230222_m1; *PEG10*, Hs00248288_s1; *POT1*, Hs00209984_m1; *GATA3*, Hs00231122_m1; *IGFBP7*, Hs00266026_m1; ID4, *SEMA3B*, Hs00190328_m1.

**Analysis of DNA copy numbers in breast cancers.** Real-time PCR to determine genomic DNA copy numbers was carried out using an ABI PRISM 7900HT Sequence Detection System (Applied Biosystems); information on the PCR primers is available on request. The ΔΔCt method of relative quantification using real-time quantitative PCR with SYBR Green I detection was adapted and optimized to estimate the copy numbers of five genes. In addition, the $2^{-\Delta\Delta Ct}$ method of relative quantification (described in detail in ref. 20) was adapted to estimate the copy numbers of five genes. This method, which enabled us to estimate gene copy numbers in unknown samples, had two main prerequisites. The first was the existence of at least one calibrator consisting of template DNA with a known copy number of each of the studied genes. The second was the need to have a housekeeping gene whose copy number was the same in all samples. This enables normalization of the quantitative data. In this work, albumin was used as the calibrator, whereas *GAPDH* served as the housekeeping gene in all experiments. For quantitative PCR carried out with genomic DNA, we used a cutoff ratio of 2.2 to define genomic amplification.

**Immunohistochemical and immunocytochemical analyses of PRDM14.** Formalin-fixed, paraffin-embedded sections of human breast carcinomas in 10 mmol/L sodium citrate were heated in a microwave oven at maximum power for 15 min and then at a reduced power for 15 min to achieve antigen recovery. After they were blocked in a 5% solution of bovine

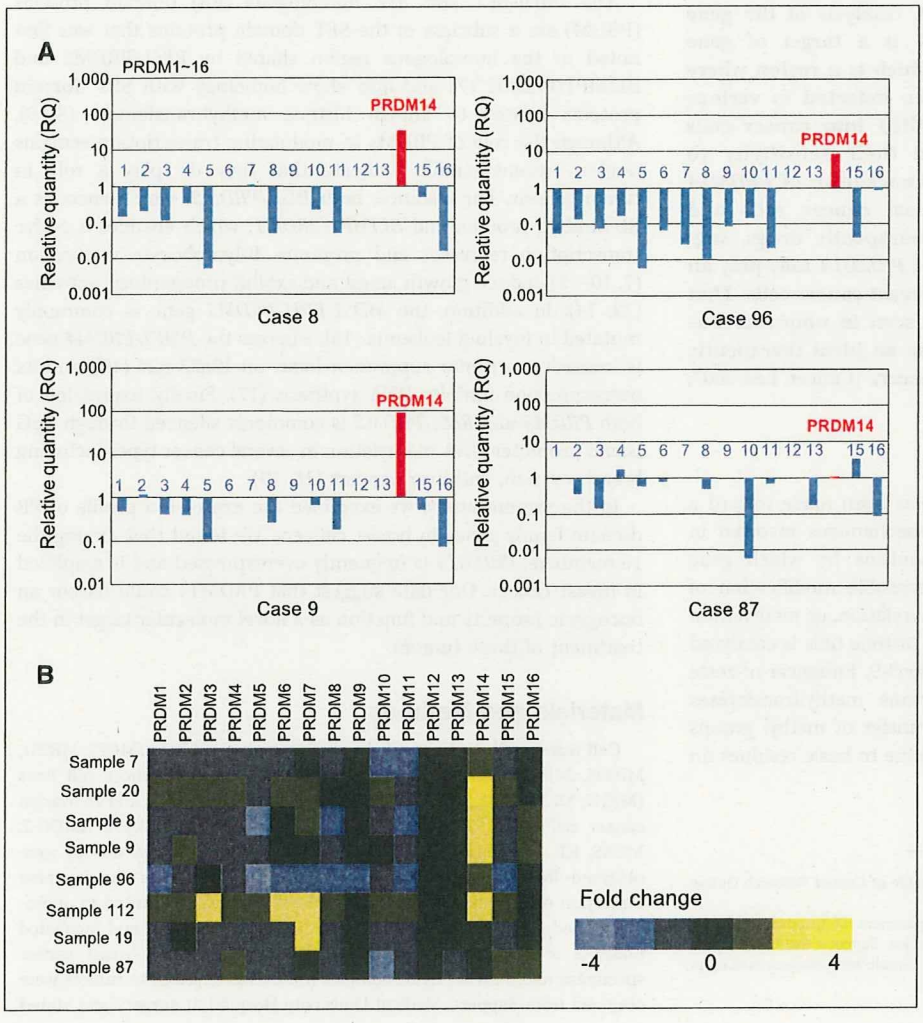


**Figure 1.** Analysis of PR domain family gene expression in breast cancer. *A*, levels of expression of *PRDM1-16* in breast cancer tissues relative to normal breast tissues were determined by real-time PCR. *Y-axis*, *PRDM14* levels in breast cancer tissue normalized to normal breast tissue. Case numbers are shown below the column. *B*, expression profile of *PRDM* family genes in breast cancer. The expression level of each *PRDM* gene in the indicated samples is shown according to a pseudocolor gradient relative to the expression in normal breast epithelium.

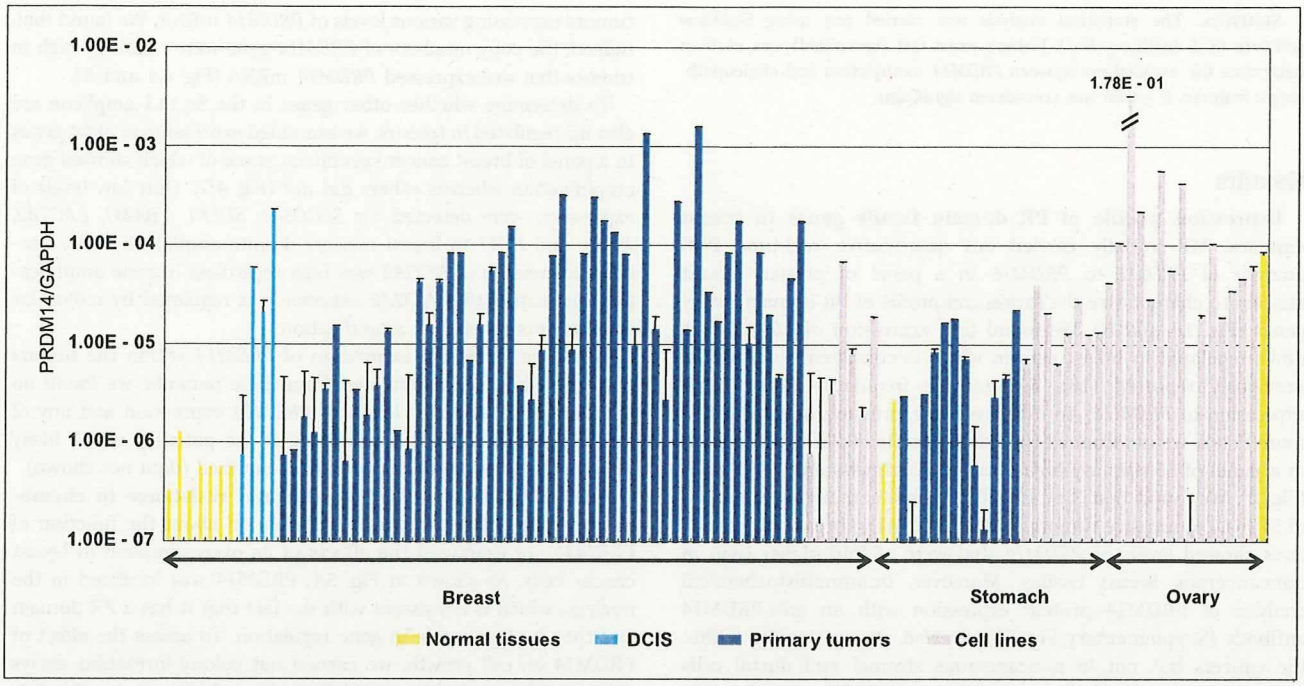


**Figure 2.** Quantitative analysis of *PRDM14* expression in various tumors and normal tissues. *Y-axis*, levels of *PRDM14* expression normalized to GAPDH. Tissue types are shown below the columns. *Columns*, mean of triplicates; *bars*, SE. *DCIS*, ductal carcinoma *in situ*.

serum albumin in PBS also containing 0.5% Tween 20, the sections were incubated with rabbit anti-human PRDM14 antibody (1:100 dilution; Abcam) overnight at 4°C. The sections were then developed using EnVision-Plus reagents (DAKO Corp.), with 3,3′-diaminobenzidine serving as the chromogen, and counterstained with hematoxylin, after which microscopic images were captured digitally. The results of PRDM14 immunostaining in breast cancers were scored independently by two pathologists (H.H. and M.S.) blinded to the protocol who concurred in the scoring.

For immunofluorescent staining of PRDM14, cells were fixed in 3.7% formalin solution for 10 min at 25°C, washed with PBS, and then incubated overnight with rabbit anti-human PRDM14 (ABGENT). The nuclei were stained with Vectashield mounting medium with 4′,6-diamidino-2-phenylindole (DAPI; Vector Laboratories, Inc.).

**Fluorescence *in situ* hybridization.** Formalin-fixed paraffin-embedded tissues were used for fluorescence *in situ* hybridization (FISH) analysis. BAC clones (RP11-152C15) containing the genomic sequences of the 8q.13.3 amplicon were purchased from Invitrogen. BAC probe was labeled using the Nick Translation method, hybridized at 37°C for 16 h, and then incubated with anti-digoxigenin-Cy3. Nuclei were stained with DAPI. Signals were detected using a fluorescence microscope (Leica CW-4000).

**Colony formation and cell growth assay.** Cells ($1 \times 10^6$) were transfected with 5 μg of pCMV-PRDM14 or pCMV-Tag2A expression vector using a Nucleofector Electroporation System (Amaxa). They were then plated in 60-mm culture dishes, selected for 14 days in medium containing G418, and stained with Giemsa. Experiments were carried out in triplicate and colonies were counted using NIH IMAGE software.

Anchorage-independent growth assays were done as previously described (21). MCF10A breast epithelial cells were transfected with mutant *H-ras*, *PRDM14*, or mutant *Ha-ras* + *PRDM14*. A layer of 1% agar in McCoy's medium was poured and allowed to solidify. Transfected cells ($1 \times 10^3$) were suspended in a 0.36% bactoagar supplemented with McCoy's 5A medium and overlaid on the agar in triplicate wells. After 3 weeks, images of the colonies were captured with an Olympus IX71 microscope using the Metaview software (Universal Imaging Corp., Molecular Devices).

To assess cell growth, 3-(4,5-dimethylthiazol-2-yl)-2,5-diphenyltetrazolium bromide (MTT) assays were carried out using SKBr-3 cells stably expressing *PRDM14*; cells transfected with pCMV-Tag2 and thus stably expressing Flag-tag served as a control. The cells ($1 \times 10^4$) were plated in 96-well plates and incubated with 50 μmol/L *cis*-diammine-dichloroplatinum (CDDP), 50 μmol/L etoposide (VP-16), 1 mmol/L docetaxel, or 200 ng/mL Adriamycin. After 48 h, cell viability was assessed in MTT assays.

**Gene expression profile in SKBr-3 cells stably expressing *PRDM14*.** Microarray experiments were carried out using the Agilent Whole Human Oligo Microarray 41K platform (Agilent Technologies). Total RNA was extracted with RNAeasy (Qiagen) from two clones stably expressing *PRDM14* and used as a template for synthesis of Cy5-labeled cDNA probes. Total RNA from SKBr-3 cells stably expressing pCMV-Tag2 vector also was labeled with Cy-3 and served as a control. The hybridized slides were scanned with a Microarray Scanner (Agilent Technologies).

**Knockdown of *PRDM14*.** For *PRDM14* knockdown studies, $1 \times 10^6$ PA-1 cells plated in 60-mm plates were transfected using an Amaxa electroporation system (Amaxa). siRNA was designed by B-Bridge International, Inc. Three siRNA sequences that target *PRDM14* were 5′-CCAGUGAAGUGAAGACCUATT-3′ (siPRDM14-1F) and 5′-UAGGUCUUCACUUCACUGGTT-3′ (siPRDM14-1R), 5′-GGACAAGGGCGAUAGGAAATT-3′ (siPRDM14-2F) and 5′-UUUCCUAUCGCCCUUGUCCTT-3′ (siPRDM14-2R), and 5′-GGGAAAAUCUUCUCAGAUCTT-3′ (siPRDM14-3F) and 5′-GAUCUGAGAAGAUUUUCCCTT-3′ (siPRDM14-3R). The sequences of the three control siRNA oligos used were 5′-ATCCGCGCGATAGTACGTA-3′ (siRNA-control-1), 5′-TTACGCGTAGCGTAATACG-3′ (siRNA-control-2), and 5′-TATTCGCGCGTATAGCGGT-3′ (siRNA-control-3). Cells were harvested after 48 h and the RNA was isolated using an RNAEasy extraction kit (Qiagen). Cell growth was assessed by counting the numbers of cells. In some instances, the cells were treated with 50 μmol/L CDDP or 1 mmol/L docetaxel 48 h after transfection. After treatment with siRNA and/or drugs, the cells were harvested, fixed in 70% ethanol, incubated with 2 mg/mL RNase, and stained in 50 μg/mL propidium iodide solution. Approximately $5 \times 10^4$ stained cells were then analyzed with a Becton Dickinson FACScan flow cytometer.

**Statistics.** The statistical analysis was carried out using StatView software (SAS Institute, Inc.). Fisher's exact test (two-sided) was used to determine the association between *PRDM14* methylation and clinicopathologic features. $P < 0.05$ was considered significant.

## Results

**Expression profile of PR domain family genes in breast cancers.** We initially carried out quantitative real-time PCR analysis of *PRDM1* to *PRDM16* in a panel of primary breast cancers to characterize the expression profile of PR domain family genes (Fig. 1*A* and *B*). We found that expression of *PRDM5* was down-regulated in breast cancer, which is consistent with results previously reported (18), whereas we frequently noted overexpression of *PRDM14*. To examine the expression of *PRDM14* in more detail, we determined the relative levels of *PRDM* expression in a panel of 55 primary breast cancer specimens and 7 cell lines (Fig. 2). We found that 3 of 4 (75.0%) ductal carcinoma *in situ*, 33 of 51 (64.7%) invasive tumors, and 4 of 7 (57.1%) breast cancer cell lines showed levels of *PRDM14* that were >5-fold higher than in noncancerous breast tissues. Moreover, immunohistochemical analysis of PRDM14 protein expression with an anti-PRDM14 antibody (Supplementary Fig. S1) revealed strong staining within the cancers but not in noncancerous stromal and ductal cells (Fig. 3). We also found that expression of *PRDM14* was often up-regulated in gastric and ovarian cancers (Fig. 2).

**Correlation between overexpression and amplification of *PRDM14*.** *PRDM14* is located on chromosome 8q in region 8q13.3, where gene amplification has frequently been observed in human tumors including those of the breast (22, 23). Therefore, to learn whether overexpression of *PRDM14* is associated with gene amplification, we used quantitative real-time PCR to determine the gene copy numbers in the region spanning 8q13-8q24 in 23 tumors expressing various levels of *PRDM14* mRNA. We found that, indeed, the copy numbers of *PRDM14* gene were relatively high in tumors that overexpressed *PRDM14* mRNA (Fig. 4*A* and *B*).

To determine whether other genes in the 8q.13.3 amplicon are also up-regulated in tumors, we examined expression of eight genes in a panel of breast cancer specimens, some of which showed gene amplification whereas others did not (Fig. 4*C*). Only low levels of expression were detected for *SLCO5A1, SULF1, TRAM1, LACTB2, XKR9,* and *EYA1* in breast cancers despite amplification. By contrast, expression of *NCOA2* was high regardless of gene amplification, indicating that *NCOA2* expression is regulated by molecular mechanisms other than amplification.

When we correlated expression of *PRDM14* within the tumors with the clinical data obtained from these patients, we found no correlation between the levels of *PRDM14* expression and any of the clinicopathologic characteristics of the patients, which likely reflects the small number of samples analyzed (data not shown).

**Role of PRDM14 in cell growth and resistance to chemotherapeutic drugs.** To obtain information about the function of PRDM14, we examined the effects of its overexpression in breast cancer cells. As shown in Fig. 5*A*, PRDM14 was localized in the nucleus, which is consistent with the fact that it has a PR domain and that it plays a role in gene regulation. To assess the effect of PRDM14 on cell growth, we carried out colony formation assays after transfecting MCF7 and SKBr-3 cells, which express only low levels of endogenous PRDM14, with pCMV-PRDM14 or pCMV-Tag2A. Following transfection, cells expressing PRDM14 showed markedly higher numbers of colonies than cells expressing Flag-tag (a result that was confirmed in three independent experiments; Fig. 5*B*). In addition, anchorage-independent growth assays using two independent clones stably expressing PRDM14 revealed that overexpression of PRDM14 enhances the ability of cells to grow without first attaching to a substrate (Supplementary Fig. S2).

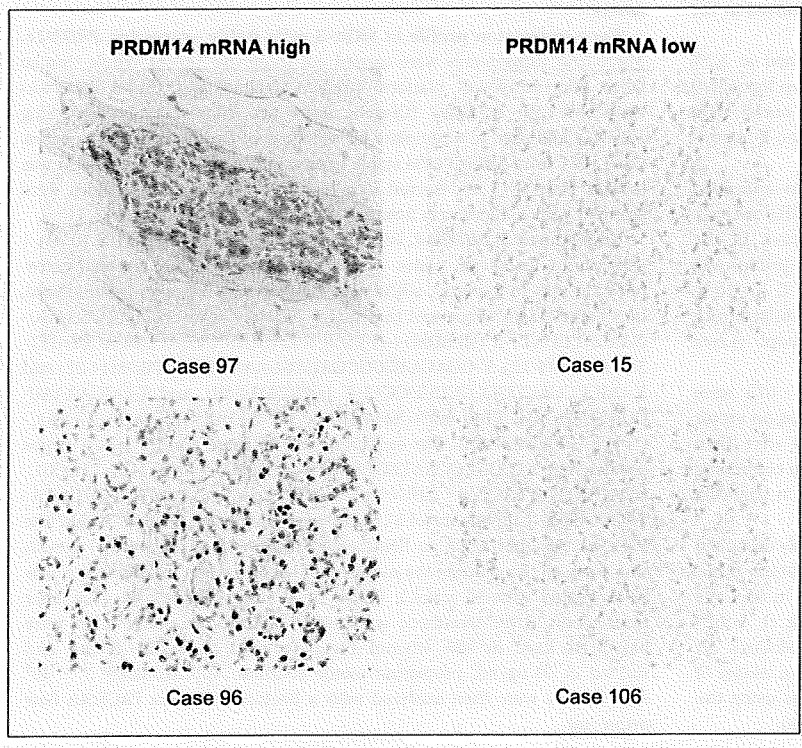


**Figure 3.** Representative results of immunohistochemical staining of PRDM14 in breast cancer tissues. *Left,* breast cancer specimens expressing high levels of PRDM14 mRNA (cases 97 and 96); *right,* specimens expressing low or negligible levels of PRDM14 mRNA (cases 15 and 106).

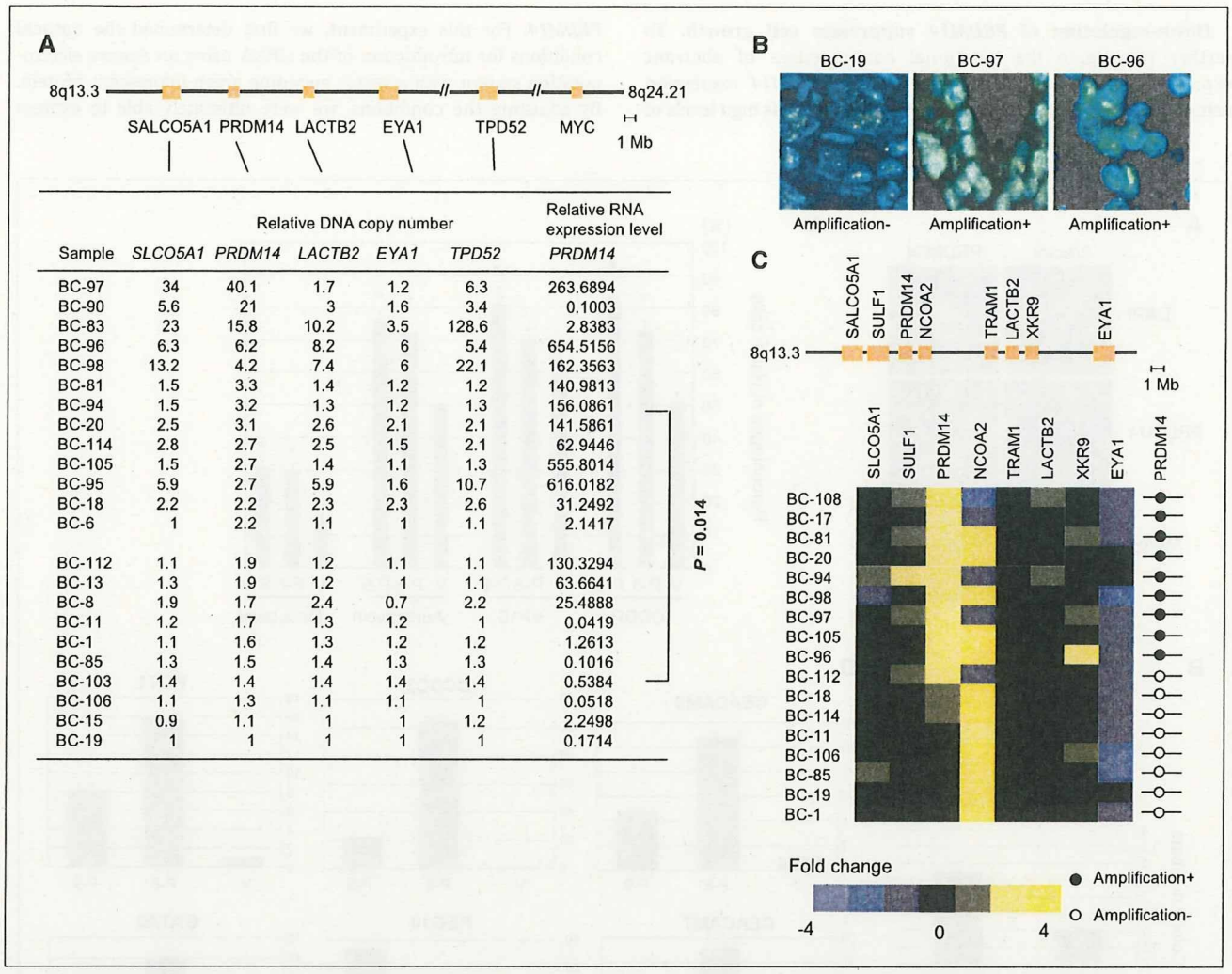


| Sample | Relative DNA copy number *SLCO5A1* | *PRDM14* | *LACTB2* | *EYA1* | *TPD52* | Relative RNA expression level *PRDM14* | |
|---|---|---|---|---|---|---|---|
| BC-97 | 34 | 40.1 | 1.7 | 1.2 | 6.3 | 263.6894 | |
| BC-90 | 5.6 | 21 | 3 | 1.6 | 3.4 | 0.1003 | |
| BC-83 | 23 | 15.8 | 10.2 | 3.5 | 128.6 | 2.8383 | |
| BC-96 | 6.3 | 6.2 | 8.2 | 6 | 5.4 | 654.5156 | |
| BC-98 | 13.2 | 4.2 | 7.4 | 6 | 22.1 | 162.3563 | |
| BC-81 | 1.5 | 3.3 | 1.4 | 1.2 | 1.2 | 140.9813 | |
| BC-94 | 1.5 | 3.2 | 1.3 | 1.2 | 1.3 | 156.0861 | |
| BC-20 | 2.5 | 3.1 | 2.6 | 2.1 | 2.1 | 141.5861 | |
| BC-114 | 2.8 | 2.7 | 2.5 | 1.5 | 2.1 | 62.9446 | |
| BC-105 | 1.5 | 2.7 | 1.4 | 1.1 | 1.3 | 555.8014 | |
| BC-95 | 5.9 | 2.7 | 5.9 | 1.6 | 10.7 | 616.0182 | |
| BC-18 | 2.2 | 2.2 | 2.3 | 2.3 | 2.6 | 31.2492 | |
| BC-6 | 1 | 2.2 | 1.1 | 1 | 1.1 | 2.1417 | |
| BC-112 | 1.1 | 1.9 | 1.2 | 1.1 | 1.1 | 130.3294 | |
| BC-13 | 1.3 | 1.9 | 1.2 | 1 | 1.1 | 63.6641 | |
| BC-8 | 1.9 | 1.7 | 2.4 | 0.7 | 2.2 | 25.4888 | |
| BC-11 | 1.2 | 1.7 | 1.3 | 1.2 | 1 | 0.0419 | |
| BC-1 | 1.1 | 1.6 | 1.3 | 1.2 | 1.2 | 1.2613 | |
| BC-85 | 1.3 | 1.5 | 1.4 | 1.3 | 1.3 | 0.1016 | |
| BC-103 | 1.4 | 1.4 | 1.4 | 1.4 | 1.4 | 0.5384 | |
| BC-106 | 1.1 | 1.3 | 1.1 | 1.1 | 1 | 0.0518 | |
| BC-15 | 0.9 | 1.1 | 1 | 1 | 1.2 | 2.2498 | |
| BC-19 | 1 | 1 | 1 | 1 | 1 | 0.1714 | |

$P = 0.014$

**Figure 4.** Amplification of PRDM14 in breast cancers. *A*, relative copy numbers of five genes located around the PRDM14 locus and the relative expression levels of PRDM14. The loci examined are shown on the top. Expression of PRDM14 was significantly higher in tumors with gene amplification than in those without amplification ($P = 0.014$). *B*, FISH analysis. Validation of 8q13.3 amplification was carried out using FISH analysis in three representative specimens using a probe located at 8q13.3. *C*, expression profile of the 8q13.3 amplicon in breast cancers. Real-time PCR was carried out for eight genes located in the 8q13.3 region. The expression level of each gene in the indicated samples is shown according to a pseudocolor gradient relative to the expression in normal breast epithelium. ●, amplification; ○, no amplification. Sample numbers are shown on the left.

Apparently, overexpression of PRDM14 leads to increased breast cancer cell growth.

We then assessed the capacity of PRDM14 to mediate resistance to chemotherapeutic drugs by treating stable PRDM14 transfectants with CDDP, VP-16, Adriamycin, or docetaxel. As shown in Fig. 5*C*, cells stably expressing PRDM14 were significantly more resistant to the drugs than cells expressing Flag-tag.

**Identification of genes regulated by PRDM14.** Because PRDMs are involved in the regulation of gene transcription, we next used a microarray to examine the effect of overexpressing PRDM14 on gene expression and compiled a list of PRDM14-responsive genes. These genes were defined as exhibiting a >3-fold up-regulation or 2-fold down-regulation in the presence of PRDM14 (PRDM14-transfected SKBr-3/pCMV-Tag2–transfected SKBr-3 ratio). We found that overexpression of PRDM14 led to up-regulation of 116 genes and down-regulation of 107 genes in both the SK-P8 and SK-P9 clones (Supplementary Tables S1 and S2). These results were confirmed by real-time PCR, which showed that the expression levels of *CEACAM6, CEACAM7, CCDC3, PEG10, POT1,* and *GATA3* were all significantly higher in cells stably expressing PRDM14 than in cells expressing pCMV-Tag2. Conversely, expression of *IGFBP7, ID4,* and *SEMA3B* was significantly down-regulated in SKBr-3 cells stably expressing PRDM14 (Fig. 5*D*).

**Enhancement of Ha-ras–induced transformation of MCF10A cells by PRDM14.** To assess the effect of overexpression of PRDM14 in untransformed cells, we evaluated the capacity of PRDM14 to induce transformation of MCF10A breast epithelial cells. As previously observed (21), transfection of MCF10A cells with activated H-ras induced cell proliferation and colony formation in soft agar. By contrast, introduction of PRDM14 into MCF10A cells did not induce proliferation, but it did enhance the growth induced by activated Ha-ras (Fig. 6*A* and *B*). Thus, PRDM14 seems to act in concert with a growth signal to facilitate cellular transformation.

**Down-regulation of *PRDM14* suppresses cell growth.** To further investigate the functional consequences of aberrant expression of *PRDM14*, we knocked down *PRDM14* expression using siRNA in PA-1 cells, which constitutively express high levels of *PRDM14*. For this experiment, we first determined the optimal conditions for introduction of the siRNA using an Amaxa electroporation system with a vector encoding green fluorescent protein. By adjusting the conditions, we were ultimately able to express

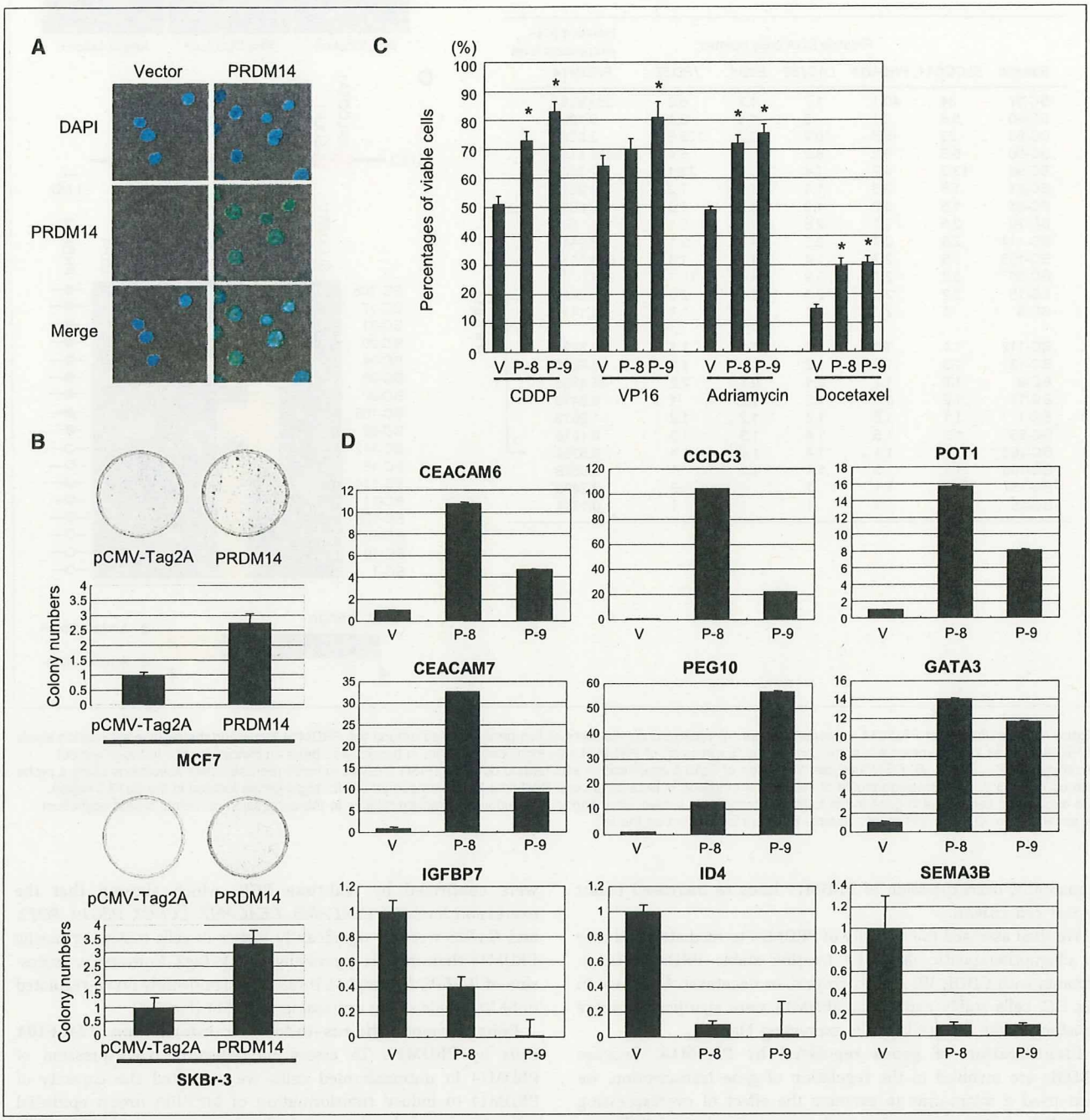


**Figure 5.** Oncogenic activity of PRDM14. *A,* immunofluorescence analysis of PRDM14 in breast cancer cells. SKBr-3 cells were transfected with pCMV-Tag2A or pCMV-PRDM14 and then labeled with anti-PRDM14 antibody. The nucleus was stained with DAPI. *B,* overexpression of PRDM14 enhances colony growth of breast cancer cells. MCF7 and SKBr-3 cells were transfected with either pCMV-Tag2A (control plasmid encoding Flag-tag) or pCMV-PRDM14 and then selected by incubation with 0.7 mg/mL G418. After 14 d, plates were stained with Giemsa solution and the colonies were counted. *C,* ectopic expression of PRDM14 reduces the sensitivity of SKBr-3 cells to chemotherapeutic drugs. Two clones [SKBr-3-PRDM14-8 (*P-8*) and SKBr-3-PRDM14-9 (*P-9*)] showing stable expression of PRDM14 driven by the CMV promoter were established. The cells were then treated with 50 μmol/L CDDP, 50 μmol/L VP-16, 0.2 mg Adriamycin, or 1 μmol/L docetaxel for 48 h, after which cell viability was assessed by MTT assays. *Columns,* mean from three independent experiments; *bars,* SE; *, $P < 0.01$, versus control [SKBr-3-pCMV-Tag2A (*V*)]. *D,* real-time PCR analysis confirming the results of the microarray analysis. Expression of putative PRDM14 target genes was examined using cDNA from two clones stably expressing PRDM14 (*P-8* and *P-9*). One clone stably expressing Flag-tag served as a control (*V*).

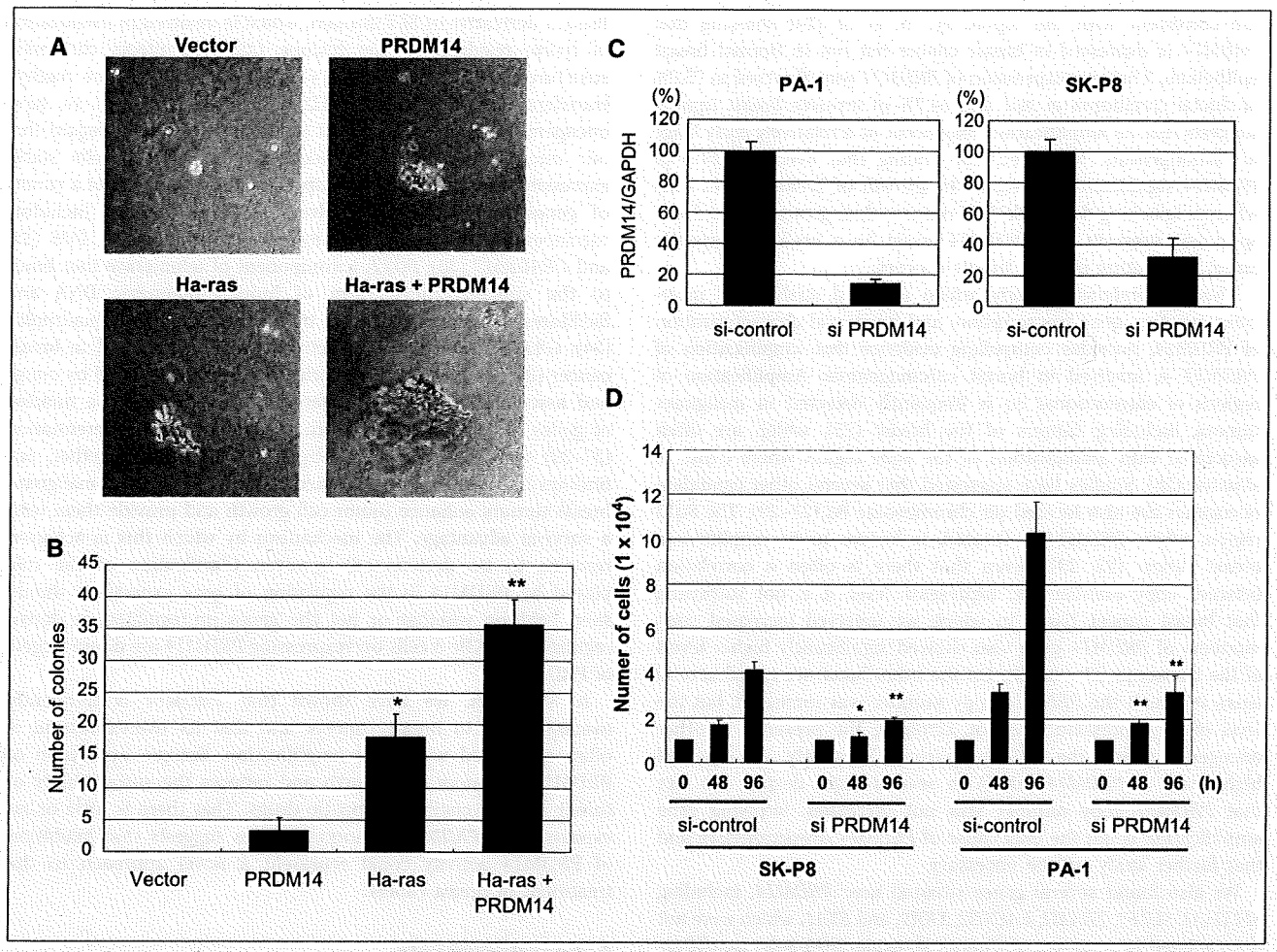


**Figure 6.** Role of PRDM14 in cell transformation, growth, and apoptosis. *A,* PRDM14 enhanced Ha-ras–induced anchorage-independent growth of MCF10A cells. MCF10A cells were transfected with mutant Ha-ras, PRDM14, or mutant Ha-ras + PRDM14 and then plated in soft agar. After incubation for 3 wk, colonies were analyzed by Metaview software. *B,* numbers of colonies of Ha-ras, PRDM14, and Ha-ras + PRDM14 transfectants were counted. *Columns,* mean from three independent experiments; *bars,* SE; *, $P < 0.05$; **, $P < 0.01$. *C,* knockdown of PRDM14 by siRNA in the cancer cell lines. PA-1 and SK-P8 cells, which constitutively express high levels of PRDM14, were transfected with control or PRDM14-targeted siRNA (*si-control* and *siPRDM14*, respectively). After 48 h, the cells were harvested and expression of PRDM14 was assessed by quantitative real-time PCR. *D,* knockdown of PRDM14 suppresses cell growth. PA-1 and SK-P8 cells treated with either si-control or siPRDM14 were grown for 48 or 96 h, after which cell numbers were counted. *Columns,* mean from three independent experiments; *bars,* SE. *, $P < 0.05$; **, $P < 0.01$, versus si-control.

green fluorescent protein in ~80% of cells (data not shown). Under those optimized conditions, introduction of a mixture of three siRNA oligos targeting *PRDM14* in PA-1 cells resulted in an 85% reduction in *PRDM14* mRNA levels, as compared with cells transfected with control siRNA (Fig. 6*C*). When we then tested whether knocking down *PRDM14* would affect cell growth, we found that cell numbers were significantly diminished by transfection with *PRDM14* siRNA, as compared with transfection with control siRNA (Fig. 6*D*). Down-regulation of *PRDM14* in SKBr-3 cells overexpressing the gene also reduced cell growth (Fig. 6*D*). Expression of two *PRDM14* target genes, *CEACAM6* and *GATA3*, was also down-regulated in PA-1 cells transfected with *PRDM14* siRNA (Supplementary Fig. S3*A*). Conversely, expression of *IGFBP7* was up-regulated when *PRDM14* was knocked down. Finally, we examined the effect of knocking down *PRDM14* on the sensitivity of cells to chemotherapeutic drugs. We found that *PRDM14* knockdown induced apoptosis in PA-1 cells (Supplementary Fig. S3*B*) and also increased the susceptibility of cells to apoptosis induced by CDDP and docetaxel. The apoptotic effects of down-regulating *PRDM14* and of the two chemotherapeutic drugs were additive, however, suggesting they act via independent pathways.

## Discussion

In the present study, we analyzed the expression profiles of PR domain family genes in a panel of breast cancers. Our results indicate that expression of *PRDMs* in malignant breast tumors differs from that in normal breast tissues. For instance, we found that *PRDM5* was down-regulated in breast tumors, which is consistent with the earlier finding that *PRDM5* is methylated in breast cancers (18) and confirms that our high-throughput approach was reliable enough for valid characterization of the gene expression profile. In addition, we found that although there is little or no expression of *PRDM14* in noncancerous tissues, it was frequently overexpressed in human breast cancer tissues and that this up-regulation is associated with gene amplification. Our results

are consistent with the report by Hu et al. (24) showing that *PRDM14* is expressed in breast cancer but not in normal breast epithelium. That overexpression of *PRDM14* was observed in 75.0% of ductal carcinoma *in situ* and 64.7% of invasive breast tumors suggests that its amplification may occur at a relatively early stage of tumorigenesis. Moreover, our finding that overexpression of *PRDM14* significantly increases the growth of breast cancer cells whereas knocking down *PRDM14* reduces their growth and induces apoptosis suggests that PRDM14 could be a useful therapeutic target for treating primary breast cancers.

This comprehensive study, which included analyses of molecular genetics, gene transcription, and functional characterization of PRDM14, provides compelling evidence that amplification of *PRDM14* is involved in breast carcinogenesis. Amplification of regions of chromosome 8q is frequently detected in malignant tumors, including tumors of the breast (25), which are often associated with amplification of the 8q24 region where *c-myc* is situated (26). Studies have suggested that several other candidate oncogenes are also located on chromosome 8q (27–29). The 8q13 region, where *PRDM14* is located, is known to be amplified in breast cancer (22, 23). Given that there is often a correlation between copy number and expression level, it is not surprising that breast cancer tissue in which we detected increased copy numbers of *PRDM14* gene also showed significantly higher levels of the transcript ($P = 0.014$). On the other hand, we noted several cases in which the *PRDM14* copy number was increased, but the level of its expression was not, implying the presence of other oncogenes within the 8q13 amplicon. Conversely, we detected high levels of *PRDM14* mRNA in several cases despite the fact that *PRDM14* copy number was not increased, implying gene amplification is not the only cause of *PRDM14* overexpression and that further study will be necessary.

We also found several genes situated near *PRDM14*, including *SLCO5A1, SULF1, TRAM1, LACTB2, XKR9*, and *EYA1*, which were not up-regulated in a subset of tumors showing 8q13-8q24 amplification. In addition, our finding that expression of *NCOA2* was high regardless of gene amplification indicates that *NCOA2* expression is regulated by molecular mechanisms other than gene amplification. And given that NCOA2 is involved in estrogen receptor–mediated gene transcription, it would be interesting to know whether up-regulation of both PRDM14 and NCOA2 is a significant factor in the development and progression of breast cancer.

The molecular mechanism by which PRDM14 enhances cell growth remains unknown. PRDM14 contains a PR domain that is likely a derivative of SET domain, which is involved in methylation of lysine residues on the histone tail, and affects chromatin structure and gene expression (1). To date, two histone methyltransferases, EZH2 and SMYD3, have been shown to have oncogenic properties (30, 31). It is noteworthy in that regard that our microarray analysis revealed that in SKBr-3 cells stably expressing *PRDM14*, there was up-regulated expression of a variety of genes known to be involved in breast cancer, including carcinoembryonic antigen family genes such as *CEACAM6* (32) and *CEACAM7* (33); *POT1*, a component of telomerase that binds to the single-stranded form of human telomeric DNA and facilitates telomerase activity by disrupting the G-quadruplex (34); *GATA3*, a transcription activator highly expressed in breast cancer (35); and *PEG10*, an imprinted gene up-regulated by c-myc and associated with cell proliferation (36). Moreover, a number of genes associated with growth suppression and differentiation (37–39) were down-regulated by PRDM14. Taken together, our findings indicate that up-regulated levels of PRDM14 in malignant breast tumors enhance tumor cell growth and provide them with a survival advantage. The mechanism by which this is achieved remains to be determined, however. Clarification of the role played by PRDM14 in the regulation of gene expression should shed light on whether or not the genes up-regulated or down-regulated in SKBr-3 cells overexpressing PRDM14 are direct targets of PRDM14.

In summary, we have shown that *PRDM14* is frequently overexpressed in breast cancers and that its overexpression is often associated with gene amplification. Ectopic expression of PRDM14 enhances cell growth and reduces the susceptibility of tumor cells to chemotherapeutic drugs. That there is little or no expression of *PRDM14* in normal tissues suggests that inhibition of PRDM14 activity could represent a novel approach to the treatment of breast cancer.

## Acknowledgments

Received 11/7/2006; revised 6/1/2007; accepted 8/18/2007.

**Grant support:** Grants-in-Aid for Scientific Research on Priority Areas from the Ministry of Education, Culture, Sports, Science, and Technology (M. Toyota, K. Imai, and T. Tokino), Grants-in-Aid for Scientific Research (S) from Japan Society for Promotion of Science (K. Imai), and a Grant-in-Aid for the Third-term Cancer Control Strategy, and Grant-in-Aid for Cancer Research from the Ministry of Health, Labor, and Welfare, Japan (M. Toyota).

The costs of publication of this article were defrayed in part by the payment of page charges. This article must therefore be hereby marked *advertisement* in accordance with 18 U.S.C. Section 1734 solely to indicate this fact.

We thank Dr. William F. Goldman for editing the manuscript.

## References

1. Zhang Y, Reinberg D. Transcription regulation by histone methylation: interplay between different covalent modifications of the core histone tails. Genes Dev 2001;15:2343–60.
2. Bannister AJ, Kouzarides T. Reversing histone methylation. Nature 2005;436:1103–6.
3. Bachmann IM, Halvorsen OJ, Collett K, et al. EZH2 expression is associated with high proliferation rate and aggressive tumor subgroups in cutaneous melanoma and cancers of the endometrium, prostate, and breast. J Clin Oncol 2006;24:268–73.
4. Hamamoto R, Silva FP, Tsuge M, et al. Enhanced SMYD3 expression is essential for the growth of breast cancer cells. Cancer Sci 2006;97:113–8.
5. Frank B, Hemminki K, Wappenschmidt B, et al. Variable number of tandem repeats polymorphism in the SMYD3 promoter region and the risk of familial breast cancer. Int J Cancer 2006;118:2917–8.
6. Tsuge M, Hamamoto R, Silva FP, et al. A variable number of tandem repeats polymorphism in an E2F-1 binding element in the 5′ flanking region of SMYD3 is a risk factor for human cancers. Nat Genet 2005;37:1104–7.
7. Keller AD, Maniatis T. Identification and characterization of a novel repressor of β-interferon gene expression. Genes Dev 1991;5:868–79.
8. Schultz J, Copley RR, Doerks T, Ponting CP, Bork P. SMART: a web-based tool for the study of genetically mobile domains. Nucleic Acids Res 2000;28:231–4.
9. Rea S, Eisenhaber F, O'Carroll D, et al. Regulation of chromatin structure by site-specific histone H3 methyltransferases. Nature 2000;406:593–9.
10. Buyse IM, Shao G, Huang S. The retinoblastoma protein binds to RIZ, a zinc-finger protein that shares an epitope with the adenovirus E1A protein. Proc Natl Acad Sci U S A 1995;92:4467–71.
11. Huang S. Blimp-1 is the murine homolog of the human transcriptional repressor PRDI-BF1. Cell 1994;78:9.
12. Lin Y, Wong K, Calame K. Repression of c-myc transcription by Blimp-1, an inducer of terminal B cell differentiation. Science 1997;276:596–9.
13. Turner CA, Jr., Mack DH, Davis MM. Blimp-1, a novel zinc finger-containing protein that can drive the maturation of B lymphocytes into immunoglobulin-secreting cells. Cell 1994;77:297–306.
14. He L, Yu JX, Liu L, et al. RIZ1, but not the alternative RIZ2 product of the same gene, is underexpressed in breast cancer, and forced RIZ1 expression causes $G_2$-M cell cycle arrest and/or apoptosis. Cancer Res 1998;58:4238–44.
15. Fears S, Mathieu C, Zeleznik-Le N, et al. Intergenic

splicing of MDS1 and EVI1 occurs in normal tissues as well as in myeloid leukemia and produces a new member of the PR domain family. Proc Natl Acad Sci U S A 1996;93:1642–7.
16. Yang XH, Huang S. PFM1 (PRDM4), a new member of the PR-domain family, maps to a tumor suppressor locus on human chromosome 12q23-24.1. Genomics 1999;61:319–25.
17. Chittka A, Chao MV. Identification of a zinc finger protein whose subcellular distribution is regulated by serum and nerve growth factor. Proc Natl Acad Sci U S A 1999;96:10705–10.
18. Deng Q, Huang S. PRDM5 is silenced in human cancers and has growth suppressive activities. Oncogene 2004;23:4903–10.
19. Du Y, Carling T, Fang W, et al. Hypermethylation in human cancers of the RIZ1 tumor suppressor gene, a member of a histone/protein methyltransferase superfamily. Cancer Res 2001;61:8094–9.
20. Livak KJ, Schmittgen TD. Analysis of relative gene expression data using real-time quantitative PCR and the $2(-\Delta\Delta C(T))$ method. Methods 2001;25:402–8.
21. Martinez-Lacaci I, Kannan S, De Santis M, et al. RAS transformation causes sustained activation of epidermal growth factor receptor and elevation of mitogen-activated protein kinase in human mammary epithelial cells. Int J Cancer 2000;88:44–52.
22. Fejzo MS, Godfrey T, Chen C, Waldman F, Gray JW. Molecular cytogenetic analysis of consistent abnormalities at 8q12-22 in breast cancer. Genes Chromosomes Cancer 1998;22:105–13.
23. Forozan F, Mahlamaki EH, Monni O, et al. Comparative genomic hybridization analysis of 38 breast cancer cell lines: a basis for interpreting complementary DNA microarray data. Cancer Res 2000;60:4519–25.
24. Hu M, Yao J, Cai L, et al. Distinct epigenetic changes in the stromal cells of breast cancers. Nat Genet 2005;37:899–905.
25. Struski S, Doco-Fenzy M, Cornillet-Lefebvre P. Compilation of published comparative genomic hybridization studies. Cancer Genet Cytogenet 2002;135:63–90.
26. Afify A, Bland KI, Mark HF. Fluorescent in situ hybridization assessment of chromosome 8 copy number in breast cancer. Breast Cancer Res Treat 1996;38:201–8.
27. Clancy JL, Henderson MJ, Russell AJ, et al. EDD, the human orthologue of the hyperplastic discs tumour suppressor gene, is amplified and overexpressed in cancer. Oncogene 2003;22:5070–81.
28. Ehlers JP, Worley L, Onken MD, Harbour JW. DDEF1 is located in an amplified region of chromosome 8q and is overexpressed in uveal melanoma. Clin Cancer Res 2005;11:3609–13.
29. Tsuneizumi M, Emi M, Nagai H, et al. Overrepresentation of the EBAG9 gene at 8q23 associated with early-stage breast cancers. Clin Cancer Res 2001;7:3526–32.
30. Hamamoto R, Furukawa Y, Morita M, et al. SMYD3 encodes a histone methyltransferase involved in the proliferation of cancer cells. Nat Cell Biol 2004;6:731–40.
31. Varambally S, Dhanasekaran SM, Zhou M, et al. The polycomb group protein EZH2 is involved in progression of prostate cancer. Nature 2002;419:624–9.
32. Poola I, Shokrani B, Bhatnagar R, et al. Expression of carcinoembryonic antigen cell adhesion molecule 6 oncoprotein in atypical ductal hyperplastic tissues is associated with the development of invasive breast cancer. Clin Cancer Res 2006;12:4773–83.
33. Ohlsson L, Hammarstrom ML, Israelsson A, et al. Biomarker selection for detection of occult tumour cells in lymph nodes of colorectal cancer patients using real-time quantitative RT-PCR. Br J Cancer 2006;95:218–25.
34. Loayza D, De Lange T. POT1 as a terminal transducer of TRF1 telomere length control. Nature 2003;423:1013–8.
35. Hoch RV, Thompson DA, Baker RJ, Weigel RJ. GATA-3 is expressed in association with estrogen receptor in breast cancer. Int J Cancer 1999;84:122–8.
36. Li CM, Margolin AA, Salas M, et al. PEG10 is a c-MYC target gene in cancer cells. Cancer Res 2006;66:665–72.
37. Burger AM, Zhang X, Li H, et al. Down-regulation of T1A12/mac25, a novel insulin-like growth factor binding protein related gene, is associated with disease progression in breast carcinomas. Oncogene 1998;16:2459–67.
38. Castro-Rivera E, Ran S, Thorpe P, Minna JD. Semaphorin 3B (SEMA3B) induces apoptosis in lung and breast cancer, whereas VEGF165 antagonizes this effect. Proc Natl Acad Sci U S A 2004;101:11432–7.
39. Yu L, Liu C, Vandeusen J, et al. Global assessment of promoter methylation in a mouse model of cancer identifies ID4 as a putative tumor-suppressor gene in human leukemia. Nat Genet 2005;37:265–74.

# PRDM5 Identified as a Target of Epigenetic Silencing in Colorectal and Gastric Cancer

Yoshiyuki Watanabe,[1,5] Minoru Toyota,[1,2,6] Yutaka Kondo,[7] Hiromu Suzuki,[2,3] Takashi Imai,[1,4] Mutsumi Ohe-Toyota,[1] Reo Maruyama,[1,2] Masanori Nojima,[2,3] Yasushi Sasaki,[1] Yoshitaka Sekido,[7] Hiroyoshi Hiratsuka,[4] Yasuhisa Shinomura,[2] Kohzoh Imai,[2] Fumio Itoh,[5] and Takashi Tokino[1]

**Abstract**

**Purpose:** PR (PRDI-BF1 and RIZ) domain proteins (PRDM) are a subfamily of the kruppel-like zinc finger gene products that play key roles during cell differentiation and malignant transformation. The aim of the present study was to begin to examine the involvement of epigenetic alteration of PRDM expression in gastric and colorectal cancer.

**Experimental Design:** We used real-time PCR to assess expression of PRDM1-17. In addition, we used bisulfite PCR to assess DNA methylation and chromatin immunoprecipitation to assess histone modification in colorectal and gastric cancer cell lines lacking PRDM5 expression.

**Results:** Among the 17 PRDM family genes tested, we found that *PRDM5* is the most frequently silenced in colorectal and gastric cancer cell lines. Silencing of PRDM5 was mediated by either DNA methylation or trimethylation of $Lys^{27}$ of histone H3. Introduction of PRDM5 into cancer cells suppressed cell growth, suggesting that it acts as a tumor suppressor in gastrointestinal cancers. Methylation of PRDM5 was detected in 6.6% (4 of 61) of primary colorectal and 50.0% (39 of 78) of primary gastric cancers but not in noncancerous tissue samples collected from areas adjacent to the tumors.

**Conclusions:** Our data suggest that epigenetic alteration of PRDM5 (e.g., methylation of its 5′-CpG island or trimethylation of $Lys^{27}$ of histone H3) likely plays a key role in the progression of gastrointestinal cancers and may be a useful molecular marker.

Epigenetic inactivation of tumor suppressor genes is frequently associated with the development and progression of human cancers (1, 2). One such epigenetic change is cytosine methylation, which leads to recruitment of transcriptional repressors and chromatin modification. During the development and progression of gastrointestinal cancer, genes involved in cell cycle regulation (3, 4), apoptosis (5, 6), DNA repair (7, 8), immune function (9), and signal transduction (10–12) are all silenced by aberrant methylation of the 5′-regions of CpG islands. Recent studies also have shown that gene silencing by DNA methylation is linked to histone modification. For example, deacetylation of histones H3 and H4 and dimethylation of lysine (K) 9 residues of histone H3 play important roles in DNA methylation–mediated gene silencing (13–15). Another histone modification involved in gene silencing is methylation of $Lys^{27}$ of histone H3 (H3K27). This reaction is often catalyzed by the histone methyltransferase EZH2 (16), overexpression of which has been linked to various cancers, including cancers of the prostate, breast, and stomach (17–19). Little is known about the role of H3K27 methylation in cancer-related gene silencing, however.

PR (PRDI-BF1 and RIZ) domain proteins (PRDM) are a subfamily of the kruppel-like zinc finger gene products and play key roles during cell differentiation and malignant transformation. PRDM1/BLIMP1 was originally identified as a transcript that was rapidly induced during the differentiation of B lymphocytes into immunoglobulin secretory cells; its expression is characteristic of late B and plasma cell lines (20, 21), and it is mutated in diffuse large B-cell lymphoma (22). PRDM2/RIZ1 has histone methyltransferase activity (23), and its aberrant methylation has been reported in various types of cancers (24, 25). PRDM3/EVI1 and PRDM16/MEL1 are associated with translocation in hematopoietic malignancies

**Authors' Affiliations:** [1]Department of Molecular Biology, Cancer Research Institute, [2]First Department of Internal Medicine, [3]Department of Public Health, and [4]Department of Oral Surgery, Sapporo Medical University, Sapporo, Japan; [5]Division of Gastroenterology and Hepatology, Department of Internal Medicine, St. Marianna University School of Medicine, Kawasaki, Japan; [6]PRESTO, JST, Japan, Kawaguchi, Japan; and [7]Division of Molecular Oncology, Aichi Cancer Center, Nagoya, Japan

Received 2/7/07; revised 5/8/07; accepted 5/23/07.

**Grant support:** Grants-in-Aid for Scientific Research on Priority Areas from the Ministry of Education, Culture, Sports, Science, and Technology (M. Toyota, K. Imai, and T. Tokino) and a Grant-in-Aid for the Third-term Cancer Control Strategy and Grant-in-Aid for Cancer Research from the Ministry of Health, Labor, and Welfare, Japan (M. Toyota).

The costs of publication of this article were defrayed in part by the payment of page charges. This article must therefore be hereby marked *advertisement* in accordance with 18 U.S.C. Section 1734 solely to indicate this fact.

**Note:** Supplementary data for this article are available at Clinical Cancer Research Online (http://clincancerres.aacrjournals.org/).

**Requests for reprints:** Minoru Toyota, First Department of Internal Medicine, Sapporo Medical University, South 1, West 16, Chuo-ku, Sapporo 060-8543, Japan. Phone: 81-11-611-2111, ext. 3211; Fax: 81-11-618-3313; E-mail: mtoyota@sapmed.ac.jp.



doi:10.1158/1078-0432.CCR-07-0305

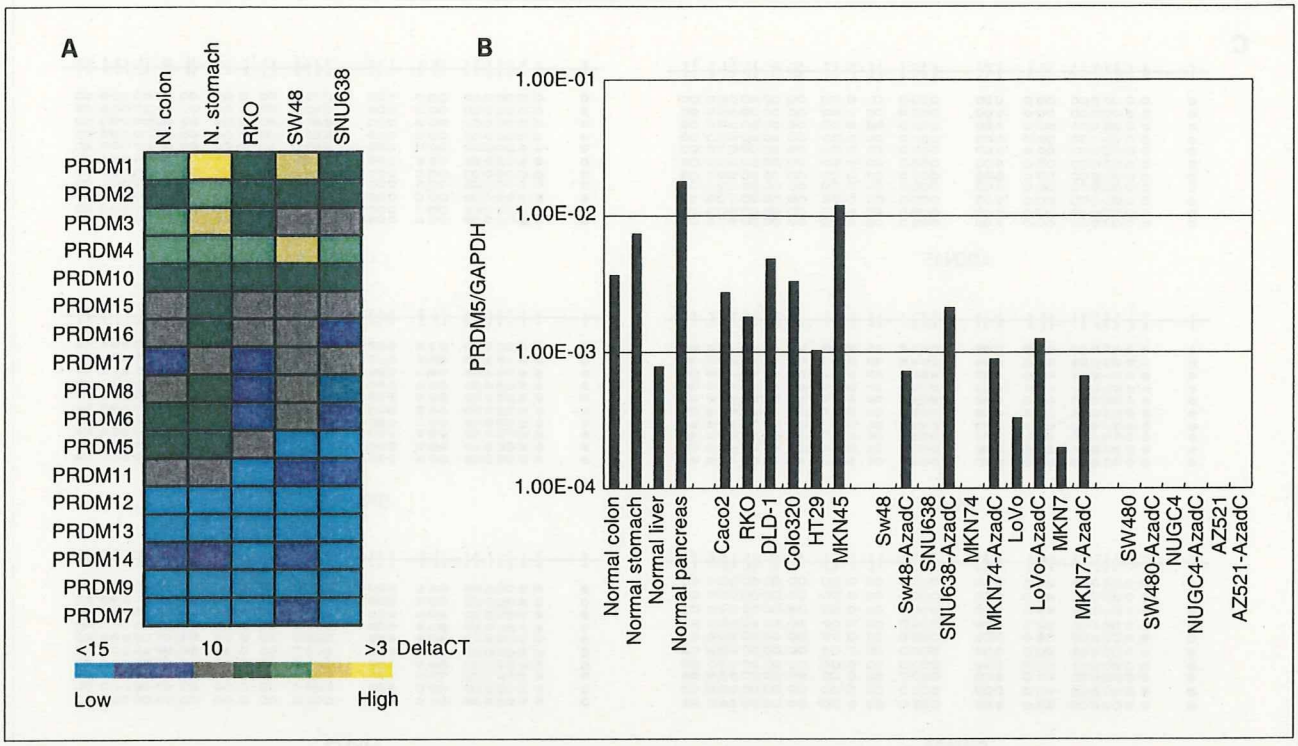


**Fig. 1.** Analysis of PRDM gene expression. *A,* heat map showing expression profiles of PRDM1-17 in normal colon, normal stomach, and three cancer cell lines. Levels of PRDM expression are normalized to glyceraldehyde-3-phosphate dehydrogenase (*GAPDH*). *B,* expression of PRDM5 in a panel of colorectal and gastric cancer cell lines. Using real-time PCR, expression of PRDM5 was analyzed in specimens from four normal tissues (colon, stomach, pancreas, and liver), eight colorectal cancer cell lines, and six gastric cancer cell lines. In eight cell lines that expressed PRDM5 at barely detectable levels, expression after treatment with 5-aza-dC also is shown.

(26, 27), and aberrant methylation and silencing of PRDM5 have been detected in both breast and liver tumors (28). In the present study, therefore, we used quantitative real-time PCR to examine the expression profile of 17 PRDM family genes in panels of gastric and colorectal cancer cell lines and primary cancer specimens. Taken together, our results suggest that epigenetic silencing of PRDM5 is a frequent event in gastrointestinal cancer, particularly in gastric cancer, and could be a useful molecular target for diagnosis and therapy.

## Materials and Methods

*Cell line and specimens.* Eight colorectal (CaCo2, RKO, SW48, DLD1, LoVo, Colo320, HT29, and SW480) and six gastric cancer cell lines (MKN7, MKN45, MKN74, AZ521, NUGC4, and SNU638) were obtained from the Japanese Collection of Research Bioresources or the American Type Culture Collection. In addition, samples of 61 primary colorectal and 78 primary gastric cancers and 44 samples of stomach mucosa collected from areas adjacent to tumors were obtained from the Department of Surgery, Sapporo Keiyukai Hospital and the Division of Gastroenterology and Hepatology, Department of Internal Medicine, St. Marianna University School of Medicine Hospital after acquisition of informed consent from each patient. All cell lines were cultured in the appropriate medium. DNA was extracted using the phenol-chloroform method, and total RNA was extracted using Isogen (Nippon Gene) according to the manufacturer's instructions. To assess restoration of PRDM5 expression, cell lines were incubated for 72 h with 2 μmol/L 5-aza-2′-deoxycytidine (5-aza-dC; Sigma), a methyltransferase inhibitor. The cells were then harvested, and total RNA was extracted for further analysis.

*Reverse transcription-PCR.* First-strand cDNA was prepared by reverse transcription of 5 μg samples of total RNA using SuperScript III reverse transcriptase (Invitrogen). The primer sequences used were 5′-ATGTGGGAGGTTCGTGGGAGTAAG-3′ (PRDM5-forward) and 5′-TTTCTGCCCGCTGTTGATTGTCT-3′ (PRDM5-reverse). The PCR protocol for reverse transcription-PCR was 95°C for 5 min, followed by 35 cycles of 1 min at 95°C, 1 min at 55°C, and 1 min at 72°C, and then a 7-min final extension at 72°C. Controls consisted of RNA treated identically but without the addition of reverse transcriptase. The integrity of the cDNA was confirmed by amplifying glyceraldehyde-3-phosphate dehydrogenase as described previously (29). Samples (10 μL) of the amplified products were subjected to 2.5% agarose gel electrophoresis and stained with ethidium bromide.

Real-time quantitative reverse transcription-PCR was carried out using Taqman Gene Expression Assays [PRDM1, Hs00153357_m1; PRDM2, Hs01030716_m1; PRDM3, Hs00602795_m1; PRDM4, Hs000973632_m1; PRDM5, Hs00218855_m1; PRDM6, Hs01372996_m1; PRDM7, Hs00364862_m1; PRDM8, Hs00220274_m1; PRDM9, Hs00360639_m1; PRDM10, Hs00999748_m1; PRDM11, Hs00220293_m1; PRDM12, Hs00222080_m1; PRDM13, Hs00222082_m1; PRDM14, Hs01119056_m1; PRDM15, Hs01562117_m1; PRDM16, Hs00223161_m1; PRDM17, Hs01119928_g1; EZH2, Hs_00544830_ml; and glyceraldehyde-3-phosphate dehydrogenase, Hs_00266705_gl (Applied Biosystems)] with a 7900HT Fast Real-time PCR System (Applied Biosystems) according to the manufacturer's instructions. 'SDS2.1 software

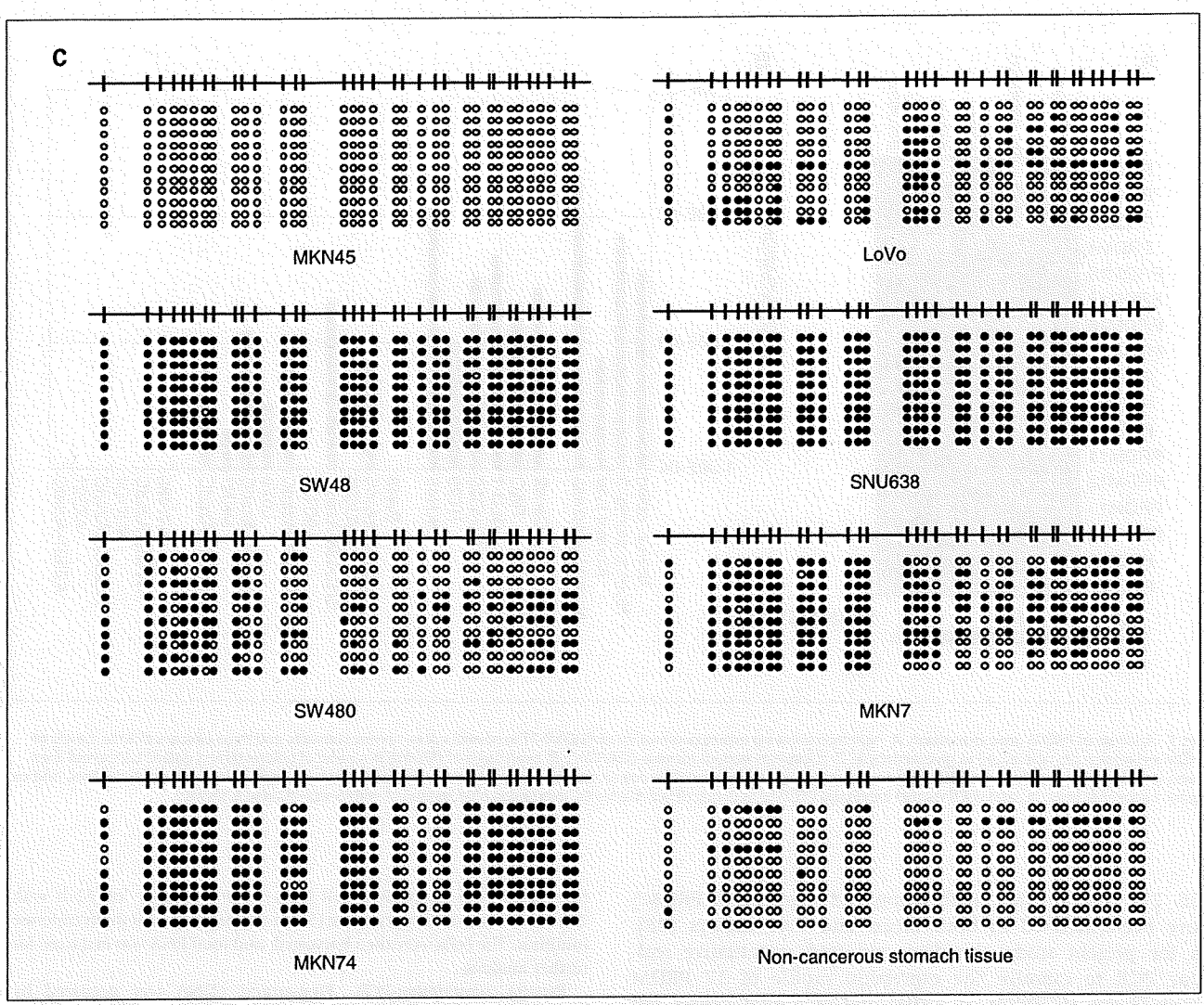


**Fig. 1** *Continued. C,* bisulfite sequence analysis of PRDM5 in the indicated colorectal and gastric cancer cell lines. Ten clones were sequenced for each cell line. White and black circles, unmethylated and methylated alleles, respectively.

(Applied Biosystems) was used to do comparative $\Delta C_t$ analysis. Glyceraldehyde-3-phosphate dehydrogenase served as an endogenous control.

***Combined bisulfite restriction analysis and bisulfite sequencing.*** Genomic DNA was initially treated with sodium bisulfite (Sigma) as described previously (30). Combined bisulfite restriction analysis (COBRA), a semiquantitative methylation assay, was then carried out as described previously (31). Touchdown PCR was then carried out as follows. After denaturing at 94°C for 3 min, the cycling protocol entailed 3 cycles of 94°C for 30 s, 58°C for 30 s, and 72°C for 30 s; 4 cycles of 94°C for 30 s, 56°C for 30 s, and 72°C for 30 s; 5 cycles of 94°C for 30 s, 54°C for 30 s, and 72°C for 30 s; and 26 cycles of 94°C for 30 s, 52°C for 30 s, and 72°C for 30 s. Primers were designed based on the nucleotide sequence obtained from Genbank. The primers used for COBRA were 5′-GGTTYGGATTYGTTTTTGTTAT-3′ (forward) and 5′-CCRCATTTAAAACCCTAAAATCA-3′ (reverse; PRDM5 GM1-R). The PCR products were digested with the restriction endonuclease *Hin*f (TaKaRa) and precipitated with ethanol, after which the resultant DNA fragments were subjected to 2.5% agarose gel electrophoresis and stained with ethidium bromide.

To sequence the bisulfite PCR products, amplified fragments were cloned into pcDNA2.1 vector using a TOPO-TA cloning kit (Invitrogen). The primer sequences used were 5′-GGTTYGGATTYGTTTTTGTTAT-3′ (forward) and 5′-AAACAAACRAAACTCCCTCACA-3′ (reverse). The cycle sequencing reaction was then carried out using a BigDye terminator kit (Applied Biosystems), and the DNA was sequenced using an ABI 3100 automated sequencer (Applied Biosystems).

***Chromatin immunoprecipitation analysis.*** Chromatin immunoprecipitation (ChIP) analysis was carried out as described previously (32). Briefly, cells were harvested and their proteins were cross-linked to DNA by incubation in 1.0% formaldehyde for 10 min at 37°C. The formaldehyde-fixed cells were allowed to settle on ice for 10 min and then spun down by brief centrifugation, after which the supernatant was carefully aspirated. The cells were then washed with ice-cold PBS containing protease inhibitors and resuspended in lysis buffer [1% SDS, 10 mmol/L EDTA, 50 mmol/L Tris-HCl

(pH8.0) and protease inhibitor]. The nucleoprotein complexes were sonicated to reduce the size of the DNA fragments to 200 to 1,000 bp and immunoprecipitated for 16 h at 4°C with 10 μL anti-K9 acetylated histone H3, anti-K9 dimethylated histone H3, anti-K27 monomethylated histone H3, or anti-K27 trimethylated histone H3 (all from Upstate Biotechnology) or anti-histone H3 antibody (as an internal control; Abcam). The resultant immune complexes were collected using protein G-Sepharose beads, after which the DNA was purified by phenol-chloroform extraction, precipitated with ethanol and resuspended in distilled water. Approximately 1:100 of the precipitated DNA was used for PCR, and 1:100 of the solution before adding antibody was used as an internal control of the quantitative accuracy of the DNA. Quantitative PCR (qPCR) was carried out using the following primers: PRDM5, 5′-CCTTCCCTGCCGGTTTCT-3′ (PRDM5-CHIP-forward), 5′-AGGCGGCACATCGAAATTT-3′ (PRDM5-CHIP-reverse), and 5′-TCTACCCTGGCACCC-3′ (PRDM5-qPCR probe); p21, GCCAACTCATTCTCCAAGTAAAAAA (p21-ChIP-forward), GTGCGCTGGACACATTTCC (p21-ChIP-reverse), and CCAGATTTGTGGCTCACT (p21-qPCR probe); p16, GGGCGGATTTCTTTTTAACAGA (p16-ChIP-forward), CGCCTGCCAGCAAAGG (p16-ChIP-reverse), and TGAACGCACTCAAAC (p16-qPCR probe); and RASSF1, GGACCCTCTTCCTCTAGCACAGT (RASSF1-ChIP-forward), GCACCACGCGGAGATACC (RASSF1-ChIP-reverse), and TGGCCTCCAGAAAC (RASSF1-qPCR-probe).

*Colony formation assays.* Cells ($1 \times 10^5$) were plated in 100-mm culture dishes for 24 h before transfection with the expression vector pcDNA3.1-PRDM5 or empty vector (5 μg each) using a Cell Line Nucleofector kit R and V (Amaxa) and a Nucleofector I electroporation device (Amaxa) according to the manufacturer's instructions. After transfection, cells were selected for 14 days in medium containing 0.6 mg/mL G418 and stained with Giemsa. The resultant colonies were then stained with crystal violet, and cells were counted in triplicate cultures using NIH Image software.

*Luciferase assay.* Three constructs (P1-P3) that covered different sized regions upstream of PRDM5 were created. All three were amplified by PCR and cloned into pCR2.1 TOPO (Invitrogen). After verification of the sequences, the fragments were ligated into pGL3-Basic vector (Promega), and cells ($5 \times 10^4$ cells in 24-well plates) were transfected using LipofectAMINE 2000 (Invitrogen). A pGL3-Basic vector without the insert served as a negative control. Forty-eight hours after transfection, luciferase activities were measured using a Dual-Luciferase Reporter Assay System (Promega).

*Knockdown of EZH2 by RNA interference.* We designed two retroviral vectors (RNAi-Ready pSIREN-RetroQ Vector, BD Biosciences) encoding a small hairpin RNA directed against EZH2 in SW480 cells (target sequences, 5′-ATATGACTGCTTCCTACAT-3′ and 5′-CATGTAGACAGGTGTATGA-3′). Both constructs reduced EZH2 expression by ~90%. As controls, we used small hairpin RNAs for the luciferase (Luc) gene synthesized by BD Biosciences or small hairpin RNA vector without the hairpin oligonucleotides (mock). Expression of EZH2 was examined using real-time PCR, after which two independent clones were used for further studies.

*Immunohistochemical analysis.* Tissue sections were deparaffinized, soaked in 10 mmol/L sodium citrate buffer, and boiled in an electronic oven for 15 min at 500 W to retrieve cell antigens. The sections were then immunohistochemically stained using the streptavidin-biotin peroxidase method (Universal DakoCytomation LSAB kit, DAKO) with primary antibodies against EZH2 (mouse anti-Ezh2 monoclonal antibody, Cell Signaling Technology, Inc.) and PRDM5 (rabbit polyclonal antibody, Abgent). Briefly, the sections were blocked in 3% $H_2O_2$ for 5 min and then incubated overnight with primary antibody at 4°C. The samples were then washed with TBS buffer and incubated with secondary antibody for 30 min.

## Results

*Epigenetic silencing of PRDM5 in colorectal and gastric cancer cell lines.* To examine the expression profile of PRDM family genes, we initially carried out real-time PCR using cDNA from normal colon and stomach tissues, two colorectal cancer cell lines (RKO and SW48), and a gastric cancer cell line (SW638). As can be seen in Fig. 1A, we detected expression of PRDM1, PRDM2, PRDM3, PRDM4 PDM10, PRDM15, PRDM16, and PRDM17 in both normal tissues and cancer cell lines; conversely, we detected little or no expression of PRDM7, PRDM9, PRDM12, PRDM13, and PRDM14 in either normal tissue or cancer cell lines. On the other hand, we detected expression of PRDM5, PRDM6, PRDM8, and PRDM11 in normal tissues but that expression was down-regulated in at least two of the three cancer cell lines tested. To further evaluate expression of these five PRDM genes, we carried out real-time PCR in a larger panel of normal tissues and colorectal and gastric cancer cell lines (Fig. 1B; Supplementary Fig. S1). We detected expression of PRDM5 in normal colon, stomach, liver, and pancreatic tissue and in six of the cell lines tested. Little or no expression was detected in eight cell lines. Treating those eight cell lines with the methyltransferase inhibitor 5-aza-dC

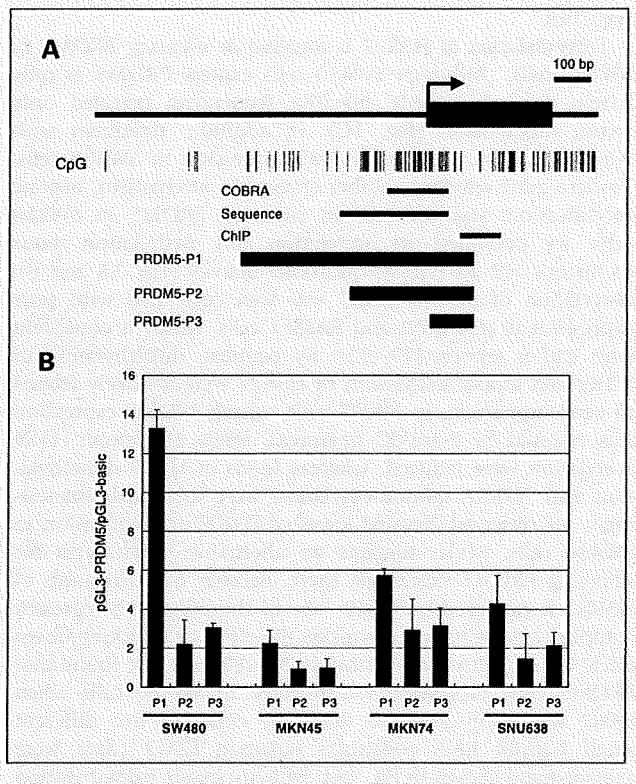


**Fig. 2.** CpG island of PRDM5 and its promoter activity in colorectal and gastric cancer cell lines. *A,* regions analyzed by COBRA, bisulfite sequencing, and ChIP assays (*horizontal bars*). Plasmid constructs containing various lengths of the 5′-flanking region of the *PRDM5* gene were cloned into pGL3-Basic vector and used for luciferase assays. *B,* luciferase assays carried out using the four cell lines shown below the columns. Values for luciferase activity were normalized by the activity in cells transfected with pGL3-Basic vector with no insert. Columns, mean ($n = 3$); bars, SD.

restored PRDM5 expression in five. In addition, levels of PRDM6, PRDM8, PRDM11, and PRDM16 expression were lower in a subset of cancer cell lines than in normal tissues, but their expression was not restored by treatment with 5-aza-dC, indicating that DNA methylation is likely not the primary mechanism by which these genes were silenced (Supplementary Fig. S1).

***Aberrant DNA methylation of PRDM5 is associated with gene silencing.*** We next used bisulfite sequencing to assess the methylation of the 5′-CpG island of PRDM5 in a panel of cancer cell lines and normal tissues (Figs. 1C and 2A). Although normal stomach tissue and MKN45 cells showed very little methylation, dense methylation in the region around the transcription start site was detected in SW48, SNU638, MKN74, and MKN7 cells, which expressed little or no PRDM5. SW480 cells showed relatively sparse methylation, and LoVo cells showed very little methylation.

We then used luciferase assays to compare the PRDM5 promoter activity in cell lines that did (MKN45) or did not (SW480, MKN74, and SNU638) express PRDM5. Three different constructs were created that covered different sized regions upstream from the transcription start site (Fig. 2A). Promoter activity was detected in all of the cell lines tested, regardless of gene expression, with most of the luciferase activity residing in the construct that contained the largest sequence (-205 to -502 bp; Fig. 2B). Thus, the silencing of PRDM5 does not seem to reflect the absence of a transcriptional regulator.

***Trimethylation of H3K27 is involved in silencing PRDM5 in SW480 cells.*** Although SW480 cells express PRDM5 at only barely detectable levels, bisulfite sequencing revealed only sparse methylation (Fig. 1C). In addition, treatment with 5-aza-dC did not restore PRDM5 expression in SW480 cells. To determine whether another epigenetic mechanism, histone modification, was involved in silencing PRDM5 in SW480 cells, we examined the acetylation and methylation status of histone H3 on PRDM5 promoter activity (Fig. 3A and B). Acetylation of histone H3K9 was well correlated with gene expression in p16, p21, and RASSF1 cells, which is consistent with earlier reports (29, 32). By contrast, dimethylation of H3K9 and monomethylation of H3K27 were inversely related to gene expression. In MKN7 cells, where PRDM5 expression was restored by 5-aza-dC treatment, levels of histone H3K9 acetylation were reduced, whereas levels of H3K9 dimethylation and H3K27 monomethylation were increased. Interestingly, we observed elevated levels of H3K27 trimethylation in SW480 cells, which suggests an alternative mechanism for silencing PRDM5 expression there. Because trimethylation of H3K27 is catalyzed by EZH2, one of the polycomb repressor complex 2 proteins, we examined the effect of knocking down EZH2 on expression of PRDM5 in SW480 cells. We found that *PRDM5* gene expression was restored in SW480 cells when EZH2 was stably knocked down by either of two different small hairpin RNA constructs targeting EZH2 (data were averaged and shown in Fig. 4A), which suggests trimethylation of H3K27 plays a key role in silencing PRDM5 expression in SW480 cells.

Because overexpression of EZH2 has been seen previously in cancer (17–19), we also carried out an immunohistochemical analysis of EZH2 expression in a panel of primary gastric cancers. We found that 9 of the 10 specimens tested

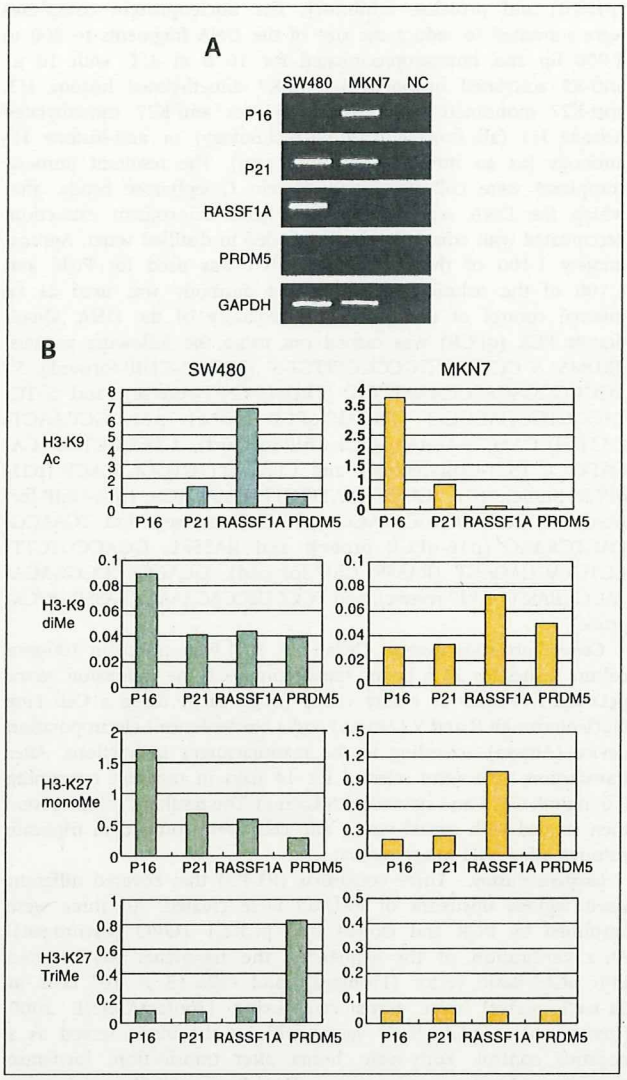


**Fig. 3.** The role of histone modification in the silencing of PRDM5. *A*, reverse transcription-PCR analysis of p16, RASSF2, p21, PRDM5, and glyceraldehyde-3-phosphate dehydrogenase expression in SW480 and MKN7 cells. NC, negative control, PCR without template. *B*, histone modification at active and silenced loci in cancers. ChIP/qPCR was used to study histone H3 modification in multiple genes in colon (SW480) and gastric (MKN7) cancer cells. Ratios of the DNA precipitated by anti-acetylated or anti-methylated H3 antibodies over that precipitated by anti-histone H3 antibody were used to calculate the relative precipitated enrichment (*Y axis*). ChIP/qPCR experiments were done at least twice, and the duplicates were highly concordant ($R = 0.97$). Antibodies used are shown on the left. The genes examined are shown below the columns. The cell lines used are shown on the top.

expressed higher levels of EZH2 than adjacent noncancerous stomach tissues (Fig. 4B), which suggests that overexpression of EZH2 is a frequent event in gastrointestinal cancer that is not always associated with down-regulation of PRDM5.

***Expression of exogenous PRDM5 suppresses cell growth in gastric cancer lines.*** We next used colony formation assays to determine whether PRDM5 has tumor suppressor activity (Fig. 5). When PRDM5 was introduced to two gastric cancer cell lines that do not otherwise express the gene,